Naval Research Laboratory
Washington, DC 20375-5000

DTIC FILE COPY

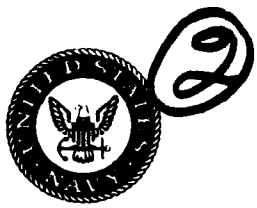

NRL Memorandum Report 6358

Sodium Fluoride Discharge for Fast Z-Pinch Experiments

B. L. WELCH,* F. C. YOUNG, R. J. COMMISSO,
D. D. HINSHELWOOD,** D. MOSHER AND B. V. WEBER**

Plasma Technology Branch
Plasma Physics Division

**University of Maryland*
College Park, MD 20742

***JAYCOR*
Vienna, VA 22180-2270

AD-A204 090

December 22, 1988

DTIC
ELECTE
S 15 FEB 1989
D
E

Approved for public release; distribution unlimited.

89 2 14 025

SECURITY CLASSIFICATION OF THIS PAGE

REPORT DOCUMENTATION PAGE

Form Approved OMB No. 0704-0188

1a. REPORT SECURITY CLASSIFICATION UNCLASSIFIED	1b. RESTRICTIVE MARKINGS
2a. SECURITY CLASSIFICATION AUTHORITY	3. DISTRIBUTION/AVAILABILITY OF REPORT Approved for public release; distribution unlimited.
2b. DECLASSIFICATION/DOWNGRADING SCHEDULE	
4. PERFORMING ORGANIZATION REPORT NUMBER(S) NRL Memorandum Report 6358	5. MONITORING ORGANIZATION REPORT NUMBER(S)
6a. NAME OF PERFORMING ORGANIZATION Naval Research Laboratory 6b. OFFICE SYMBOL (If applicable) Code 4770	7a. NAME OF MONITORING ORGANIZATION
6c. ADDRESS (City, State, and ZIP Code) Washington, DC 20375-5000	7b. ADDRESS (City, State, and ZIP Code)
8a. NAME OF FUNDING/SPONSORING ORGANIZATION SDIO IS&T Office 8b. OFFICE SYMBOL (If applicable)	9. PROCUREMENT INSTRUMENT IDENTIFICATION NUMBER
8c. ADDRESS (City, State, and ZIP Code) Washington, DC 20301-7100	10. SOURCE OF FUNDING NUMBERS PROGRAM ELEMENT NO: 63220 / PROJECT NO: / TASK NO: 80000 25RG03 / WORK UNIT ACCESSION NO: DN156-317

11. TITLE (Include Security Classification)
Sodium Fluoride Discharge for Fast Z-Pinch Experiments

12. PERSONAL AUTHOR(S)
Welch,* B.L., Young, F.C., Commisso, R.J., Hinshelwood,** D.D., Mosher, D., Weber,** B.V.

13a. TYPE OF REPORT	13b. TIME COVERED	14. DATE OF REPORT (Year, Month, Day)	15. PAGE COUNT
Interim	FROM _____ TO _____	1988 December 22	44

16 SUPPLEMENTARY NOTATION
*University of Maryland, College Park, MD 20742
**JAYCOR, Vienna, VA 22180-2270

17. COSATI CODES			18. SUBJECT TERMS (Continue on reverse if necessary and identify by block number)
FIELD	GROUP	SUB-GROUP	Capillary discharge, Plasma source Z-pinch, X-ray laser. Sodium fluoride plasma,

19. ABSTRACT (Continue on reverse if necessary and identify by block number)

A capillary-discharge plasma source has been developed to produce a sodium-bearing plasma for fast Z-pinch implosion experiments. Peak currents of 40 to 50 kA from a 0.5-kJ capacitor bank were driven through a 0.5-mm diameter, few-cm-long capillary drilled in packed solium fluoride powder to form the source. A nozzle was used to collimate plasma ejected from one end of the capillary to produce a 1 to 2-cm diameter, several-cm-long cylindrical plasma. Ions with velocities of 2.2 to 3.4 cm/μs ~~and densities of up to 5×10^{15} cm^{-3}~~ were measured with biased charge collectors located at least 5 cm from the nozzle. Measurements of visible light from neutrals near the nozzle exit gave velocities of 1.5 to 1.7 cm/μs. Indications of axial and radial nonuniformities of the plasma were observed in framing photographs of visible-light emission and in spatially-resolved spectral measurements. Neutral-sodium and neutral-fluorine lines were identified in

(Continues)

20. DISTRIBUTION/AVAILABILITY OF ABSTRACT	21. ABSTRACT SECURITY CLASSIFICATION
☒ UNCLASSIFIED/UNLIMITED ☐ SAME AS RPT. ☐ DTIC USERS	UNCLASSIFIED
22a. NAME OF RESPONSIBLE INDIVIDUAL Frank C. Young	22b TELEPHONE (Include Area Code) (202) 767-2724 22c OFFICE SYMBOL Code 4770.1

DD Form 1473, JUN 86 Previous editions are obsolete. SECURITY CLASSIFICATION OF THIS PAGE

S/N 0102-LF-014-6603

19. ABSTRACTS (Continued)

the spectral range from 2300 to 6700 Å. Also, impurity lines of carbon, copper, and hydrogen were identifed and used to characterize the plasma. Stark broadening of the Balmer alpha line of hydrogen was used to deduce a peak electron density of 8×10^{16} cm^{-3} at the exit of a 2-cm diameter nozzle. Electron temperatures of 1.4 to 1.6 eV at the nozzle exit were inferred from relative intensities of CI and CII lines. At this density and temperature, Saha-equilibrium-model calculations indicate that the plasma consists primarily of singly-ionized sodium and neutral fluorine. A total mass per unit length (sodium and fluorine) of at least 15 $\mu g/cm$ is deduced from this analysis of the plasma constituents. This capillary discharge has been used to produce 50 to 100 GW of sodium K-shell x-rays in fast Z-pinch experiments.

CONTENTS

Accession For
NTIS GRA&I
DTIC TAB
Unannounced
Justification
By
Distribution/
Availability Codes
Dist | Avail and/or Special
A-1

DTIC COPY INSPECTED

SOLIUM FLUORIDE DISCHARGE FOR FAST Z-PINCH EXPERIMENTS

I. INTRODUCTION

The possibility of creating population inversion by matched line photopumping has been suggested[1] and investigated[2,3] by a number of authors. An attractive scheme[4] employs the NaX $1s^2\ {}^1S_o$ - $1s2p\ {}^1P_1$ line at 11.0027 Å to pump the NeIX $1s^2\ {}^1S_o$ - $1s4p\ {}^1P_1$ line at 11.0003 Å. This scheme is attractive because the line coincidence is excellent (2 parts in 10^4), but it requires an intense source of 11-Å NaX pump radiation.

Intense x-ray sources are produced by Z-pinch implosions driven by fast ($\leq$ 100 ns), high-current ($\geq$ 1 MA) pulsed power generators. For example, neon gas-puff implosions driven by the Gamble II generator at the Naval Research Laboratory have produced up to 4 kJ of neon K-shell radiation with as much as 70% of the energy in the Lyman-alpha (L-α) and heliumlike resonance (He-α) lines.[5] A similar approach is being taken to produce heliumlike sodium in a Z-pinch implosion. This paper reports the development of a sodium-fluoride (NaF) capillary discharge to provide a sodium-bearing plasma for such implosion experiments. A peak power of 25 GW with a total radiated energy of 600 J has been measured in the He-α line for implosions of this NaF plasma driven by a peak current of 1.2 MA.[6] Recently, this plasma source has been used in sodium-pump/neon-lasant photopumping experiments.[7]

Discharges through dielectric capillaries that vaporize the wall are well known. They have been developed as standard light sources[8] and have been studied as plasma sources.[9] More recently, the use of capillary discharges as a soft x-ray source[10] or for thermonuclear fusion[11] has been examined. In this report, the development of a capillary discharge to produce a plasma appropriate for high-power Z-pinch implosions is described.

Manuscript approved October 17, 1988.

II. DESCRIPTION OF THE CAPILLARY SOURCE

The NaF plasma was produced by discharging a capacitor through a capillary which was drilled in packed NaF powder. The geometry of the capillary source is shown in Fig. 1. The NaF powder was supported in a Teflon (CF_2) dielectric separating the center electrode and the outer conductor. The powder was packed to a density of approximately 1 g/cm^3 in a 5-mm diameter hole in the dielectric, either 1.25 or 2.5-cm long. A 0.5-mm diameter capillary was drilled through the packed NaF powder. Previous work[1,2] with capillaries ranging in diameter from 3 to 0.3 mm indicated that more energy was coupled to the plasma when smaller diameter capillaries were used. Current was driven through the capillary from the negative high-voltage center conductor to the grounded outer conductor. Powder from the capillary walls was heated to the plasma state by the electrical discharge and subsequently ejected from the capillary by over-pressure of the heated NaF. Some measurements were also made with a CF_2 capillary which was formed by drilling a 0.5-mm diameter hole in the CF_2 dielectric.

A nozzle was used to restrict radial expansion of the plasma and to collimate the plasma into a cylindrical column. Three different anodized aluminum nozzles were used. Two nozzles had a 1.2-cm exit diameter and either a 2-cm or 5-cm length, and the other nozzle had a 2-cm exit diameter and a 5-cm length.

III. ELECTRICAL MEASUREMENTS

The current waveform of the capacitor discharge was measured to determine the electrical characteristics of the discharge. A schematic diagram of the discharge circuit is given in Fig. 2. The 1.8-μF capacitor was charged to 25 kV providing a 560-J energy store. The current waveform was modeled by an RLC circuit, and the resistance, inductance, and amplitude of the current were determined by fitting the calculated waveform to the measured current. The

capillary was initially replaced by a short circuit to determine the resistance (R) and inductance (L) of the driving circuit. The short circuit was made by replacing the NaF with a 3.2-mm diameter brass rod. Once values of R and L were known, the waveform of the current through the NaF capillary gave an indication of the total resistance ($R+R_c$) and inductance ($L+L_c$) of the circuit with a capillary load. Figure 3 presents waveforms for (i) the capillary replaced by a short circuit, (ii) a 1.25-cm long NaF capillary, and (iii) a 2.5-cm long NaF capillary. For the short-circuit load, the current oscillates in an underdamped fashion and the waveform is in good agreement with the RLC circuit-model current. With a NaF capillary load, the current is further damped due to the additional resistance of the capillary. The agreement with the RLC-model current is not as good with a capillary load because the resistance and inductance of the capillary are time dependent. Even so, the RLC-model current agrees with the measured waveform over three-fourths of the first period of the current.

The circuit characteristics obtained from the RLC model with and without NaF loads are given in Table I. The 1.25-cm capillary adds 33 mΩ and 25 nH to the circuit, while the 2.5-cm capillary adds 77 mΩ and 54 nH. The uncertainties in these resistance and inductance determinations of ± 20 mΩ and ± 20 nH,

TABLE I

RLC CIRCUIT CHARACTERISTICS FOR VARIOUS CAPILLARY CONFIGURATIONS

Configuration	$R+R_c$ (mΩ)	$L+L_c$ (nH)	Peak Current (kA)	First Period (μs)
Short-circuit capillary ($R_c=L_c=0$).	75	135	77	3.1
1.25-cm NaF capillary.	108	160	53	3.5
2.5-cm NaF capillary.	152	189	41	3.9

respectively, are based on estimating the goodness of the fits to the measured current waveforms. The scaling of the resistance with the length of the capillary is consistent with interpreting this resistance as the capillary-plasma resistance. The scaling of the inductance with the length of the capillary suggests that this inductance is associated with the current path in the capillary plasma. However, if the 25-nH increase in inductance observed for the 1.25-cm capillary arises from a linear current path in the capillary, the current must be confined to an unrealistically small diameter (0.2 μm). The large increases in inductance observed with the capillary loads are not understood. Possible explanations are that the current path in the capillary is much longer than the length of the capillary, for example, either a spiral path within the capillary, or current distributed in plasma within the exit nozzle.

The energy delivered to the capillary was determined by using the measured current and resistance to calculate the ohmic power dissipated in the capillary. Integrating this power in time gave the energy coupled to the capillary. This energy is 180 $\pm$ 50 J for the 2.5-cm capillary and 50 to 200 J for the 1.25-cm capillary. The uncertainties in these values are due to the uncertainties in the resistance determinations. More than 90% of the energy is delivered to the capillary during the first period of the current pulse.

IV. FARADAY CUP MEASUREMENTS

Faraday cups were used to determine the net ion-current density of the plasma from the capillary as a function of time. Negatively biased (50 V) cups with 0.25-mm diameter entrance apertures were placed in the vacuum chamber opposite the capillary source as shown in Fig. 4. The measured signals gave an indication of the local positive-ion current density as a function of time. By using two Faraday cups at different distances, an ion drift velocity was determined from the time difference between the signals at the two different

locations on the same shot. The velocity can also be determined by varying the distance between the Faraday cups and the capillary on multiple shots. Faraday-cup signals (see Fig. 5) were obtained for a 2.5-cm long NaF capillary with a 2-cm exit-diameter nozzle. The times of arrival of the three peaks of the Faraday-cup signals are plotted versus distance for these two shots along with two other shots in Fig. 6. Measurements were taken on the same shot at 10 and 15.6 cm, at 15 and 20.6 cm, and at 20 and 25.6 cm to minimize variations due to lack of reproducibility. The slopes of these plots indicate velocities of 3.4, 2.7, and 2.2 cm/μs for the three peaks with standard deviations of $\pm$ 0.2 cm/μs.

Once the velocity is known, the measured Faraday-cup signal, V, can be used to estimate the ion density according to

$$n_i = V/(evAR) \qquad (1)$$

where v is the ion velocity, A is the area of the Faraday-cup aperture, e is the electronic charge, and R (50 Ω) is the termination resistance of the Faraday-cup signal. It is assumed that the ions are singly charged, that electron emission from ion impact in the cup is negligible, and that the Faraday cup does not perturb the plasma flow. The Faraday-cup trace in Fig. 7 was measured with a detector located 5 cm in front of the nozzle. The first three peaks in this trace correspond to those in Figs. 5 and 6. The third and largest peak is associated with the 2.2-cm/μs velocity and represents a density of about 5×10^{15} cm^{-3}. Smaller densities were determined for the first two peaks. If the Faraday cup was located closer to the capillary, this signal was saturated. Increasing the detector bias to prevent saturation lead to electrical breakdown when plasma impinged on the detector. An order-of-magnitude estimate of the total number of charged particles arriving at 5 cm was made by integrating this signal in time and using the velocity associated with the largest peak. For this estimate, the area of the ion beam was assumed to be given by the diameter of the plasma at the Faraday cup as indicated by framing-camera pictures (see

Section V). If all these ions are assumed to be singly-ionized sodium, the estimated total mass of sodium is 23 μg. For comparison, the total mass of NaF powder from the capillary, determined by weighing the capillary before and after the discharge, was approximately 100 mg. Clearly, only a small fraction of the total NaF is ionized sodium. The total number of singly-ionized sodium ions corresponds to a total ionization energy of 0.5 J and a total kinetic energy of 5.6 J. These estimates indicate that only a small fraction of the energy delivered to the capillary (6 J out of 180 J) is carried by sodium ions in the plasma, and it is primarily kinetic rather than ionization energy.

V. VISIBLE LIGHT MEASUREMENTS

The light emitted from the plasma was recorded in a number of ways. Open-shutter photographs and framing-camera pictures were used to give an indication of the spatial distribution of light-emitting plasma. In Fig. 8a is an open-shutter photograph of the light from the discharge of a 1.25-cm long NaF capillary without a nozzle. For this measurement, a 50-Å bandpass filter centered at 5890 Å was used to transmit the sodium "doublet" lines at 5890 and 5896 Å. The elliptical image indicates that plasma is expanding from the capillary into less than 2π steradians.

A framing camera was used to record time-resolved images of the visible light as shown in Fig. 8b. Images were recorded for 0.2 μs at 1-μs intervals during the discharge. The frames are numbered sequentially in time, beginning in the lower left corner and ending in the upper right. The first frame begins 0.5 μs after the discharge is initiated unless otherwise specified. In all cases the capillary source is on the right. The framing-camera pictures show well defined luminosity fronts that progress from frame to frame. The discharge in Fig. 8b is for a 0.5-mm diameter capillary in a CF_2 dielectric without a NaF fill and without a nozzle. Also, the sodium "doublet" filter was not used. The

ejected plasma impinges onto two screens located 7.5 cm and 12.5 cm, respectively, from the capillary. Frame 1 shows plasma just beginning to exit the capillary. In later frames, two successive luminosity fronts are observed to expand from the capillary and interact with the screens. The luminosity at the exit of the capillary is peaking in frames 3 and 5. In frames 4 and 7, the luminosity peaks behind the first screen as plasma passes through this screen. The divergence of the ejected plasma into nearly 2π steradians is evident in these frames.

The effect of 1.2-cm and 2-cm diameter nozzles on redirecting the plasma can be seen in the photographs in Figs. 9 and 10, respectively. For the open-shutter photographs in Figs. 9a and 10a, the sodium "doublet" filter was not used because spectral measurements indicated that the total visible-light emission was predominantly from sodium. The light-emitting plasma is limited to a diameter comparable to the nozzle diameter. The emission from this plasma is axially and radially nonuniform. Near the exit of the nozzle, plasma is confined to the nozzle diameter. Several centimeters from the nozzle, the plasma appears to expand radially in a cone originating near the nozzle exit.

Framing-camera photographs for discharges with these same diameter nozzles are shown in Figs. 9b and 10b. Light is recorded in the first frame in Fig. 9b because the frame times have been delayed by 2 μs for this measurement. Radial confinement of the plasma by the nozzle can once again be seen but now with time resolution. The velocity of the luminosity front was estimated by measuring the distance the front travels between frames. For frames 3 to 5 in Fig. 9b the velocity of the luminosity front is about 1.7 cm/μs. In Fig. 10 a screen is located only 5 cm away from the nozzle. The frames in Fig. 10b show intense light coming from the outer edge of the nozzle suggesting that plasma is redirected toward the axis by the walls of the nozzle. Also shown is a cone of intense light originating on axis at the exit of the nozzle and extending toward

the screen. Both of these features are also evident in the open-shutter photograph in Fig. 10a. These photographs indicate that the capillary discharge can be used to produce a column of sodium-bearing plasma about 2-cm in diameter and at least 4-cm long as required for Z-pinch implosion experiments.

Photodiodes (EG&G Model FND-100) were used to record time histories of the light intensity in the geometry shown in Fig. 4. Flexible black tubing was used to restrict the detector viewing to a 1.8-cm length of the plasma, and a filter was used to limit the detector signal to only sodium "doublet" emission. By using two photodiodes to record the plasma light at two different distances from the nozzle exit, a velocity was determined. Figure 11 shows two photodiode traces corresponding to a 4-cm separation of the diodes. Velocities determined from the two peaks are 1.7 and 1.2 cm/μs. These velocities are up to a factor-of-two smaller than velocities deduced from the Faraday-cup measurements, but are in agreement with the velocity determined from framing photography. The 5 to 10-μs duration of the sodium-light emission combined with the measured velocities indicates that sodium from the capillary should form a column longer than the 4 cm required for implosion experiments on the Gamble II generator. The successive peaks observed with the Faraday cups and in the visible-light emission may be associated with the periodicity of the current driving the capillary.

Comparison of visible-light measurements, i.e., framing-camera pictures and a Faraday-cup signal, is made in Fig. 12. The framing duration and the timing interval are as in Figs. 8 to 10. Frame times corresponding to the bottom row of framing pictures in Fig. 12a are indicated by the dashed traces in Fig. 12b. The arrival of ions at the Faraday cup occurs before the luminous front reaches the same location. These observations indicate that the larger velocities determined from Faraday cups (which measure ions) are not associated with the smaller velocities obtained from photodiodes (which measure light mainly from

neutrals). Light is observed at the locations of the Faraday cups in Fig. 12a after the luminous front exits the nozzle. This light may be due to either reflection of light from the front of the Faraday cup or to emission from plasma which stagnates on the Faraday cup. No light emission was observed associated with the first peak in the Faraday-cup signal in either the framing images or the photodiode traces. These data suggest that the discharge produces a fast ion component followed by a slower, luminous, neutral component.

VI. VISIBLE AND NEAR UV SPECTROSCOPY

A 0.5-m spectrometer with a 1200 line/mm grating was used to study light emitted from the capillary-discharge plasma both photographically and with time resolution. The spectrometer viewed the plasma perpendicular to its exit from the nozzle, and a lens was used to image the source onto the entrance slit of the spectrometer as shown in Fig. 4. For the photographic work, the spectrum was spatially resolved in the radial direction at the exit of the nozzle. In spectral scans from 2300 to 6700 Å, lines of neutral sodium and neutral fluorine were identified, as well as impurity lines of carbon, copper, zinc, aluminum, and hydrogen. Spectral lines from NaI, for two different discharges, recorded with a 100-μm entrance slit, are compared in Fig. 13. In each case, the intense and broadened portion of the lines corresponds to the nozzle diameter. Measurements with various neutral-density filters and entrance-slit widths indicated that this line broadening is not due to over-exposure of the film. The line broadening is indicative of a higher electron density on axis than elsewhere in the plasma. The NaI emission is radially more uniform for the 1.2-cm diameter nozzle in Fig. 13b than for the 2-cm diameter nozzle in Fig. 13a. This suggests that radial variations of the electron density are less severe for the smaller diameter nozzle.

The sodium "doublet" emission, labeled 3s-3p in Fig. 13, appears to be reabsorbed at line center, which indicates that the plasma is opaque at these wavelengths. This absorption is attributed to neutral sodium in the ground state between the light-emitting sodium and the spectrometer. This reabsorption can be used to estimate a minimum sodium ground-state density in the plasma. Measurements were made of higher members of the NaI resonance series because the smaller oscillator strengths of these lines, compared to the 3s-3p line, leads to much larger minimum densities. A photomultiplier was coupled to the exit slit of the spectrometer to record the time histories of weak lines. The NaI line at 2852 Å (3s-5p) was scanned in wavelength and found to be reabsorbing at line center. Reabsorption occurred for a duration of more than 5 μs beginning about 6 μs after the start of the capillary current. To account for this absorption, an optical depth of at least unity is required, which corresponds to a minimum sodium ground-state density of about 3×10^{16} cm^{-3}.

Velocities of sodium atoms were determined by measuring the NaI line emission at two different distances from the nozzle. Time histories of the NaI line at 5890 Å, recorded at the nozzle and 5 cm from the nozzle, are shown in Fig. 14. Velocities corresponding to the two peaks in these signals are 1.7 and 1.5 cm/μs, respectively. These values agree with the velocities from the visible-light photodiode measurements.

Time histories of the CuI line at 5218 Å are presented in Fig. 15. The solid trace gives an indication of the impurity emission in a typical discharge. The dotted trace indicates the relative copper-impurity content when the hole in the brass outer electrode was covered with an aluminum insert. The dash-dot trace indicates the relative copper-impurity content when the aluminum insert was used and the brass center electrode was covered with tantalum foil. These results demonstrate that the copper impurity is from the brass electrodes and can be changed by modifying the electrodes.

The electron density, n_e, in the plasma was determined by measuring the Stark broadening of the Balmer alpha line (6563 Å) from the hydrogen impurity. Measurements of this line were carried out at the exit of the nozzle and were restricted in the direction perpendicular to the line-of-sight to within 2 mm of the axis in order to minimize uncertainties due to nonuniformities in n_e. Time histories of the intensity of this line were measured from 9 Å below line center to 7 Å above line center. Histories at seven different wavelengths at and above line center are given in Fig. 16. From these measurements, line profiles were extracted at various times during the discharge. The profiles were fit to Lorentzian functions, and the half-width at half-maximum was determined for each profile. An example of one of the profiles is shown in Fig. 17. There is no indication of self absorption in this line shape. Stark broadening is the major contributor to the 2.2-Å half-width of this line. For the various times of these measurements, the half-widths ranged from 1.0 to 3.5 Å. An instrumental width of only 0.3 Å for the 20-μm entrance slit was determined by scanning the 5461-Å line of a mercury vapor lamp. The thermal Doppler width is only 0.4 Å for a temperature of 2 eV. An upper limit on the Doppler width due to macroscopic motion was estimated to be 0.3 Å based on a velocity of 1.5 cm/μs. Therefore, the instrumental and Doppler contributions to the line widths are small and were neglected in determining n_e. The measured half-widths were compared with tabulated Stark widths[13] to determine the negative-charge density. This density is attributed to electrons, not negative ions, because the negative-ion density is negligible at the measured electron density and temperature, as will be shown. The Stark widths were evaluated for a temperature of 2 eV, based on measurements to be described. The Stark width at this temperature and density is not strongly dependent on temperature. A temperature of 1 eV would only cause a 5 to 15% decrease in this density. Values of n_e, determined from the measured line widths,[14] are given in Fig. 18

along with the time history of the line at line center. These are radially averaged electron densities at the nozzle exit. Recent calculations of Stark broadened profiles of the Balmer alpha line in this temperature and density range would imply slightly higher electron densities.[15] The uncertainty in each measurement arises from uncertainty in the line width due to shot-to-shot variations in the signal and to small signal-to-noise ratios at late time. The peak value of n_e is 8×10^{16} cm^{-3}. This peak is associated with the second peak in the Faraday-cup signal shown in Fig. 7. It was not possible to extend this measurement to later time corresponding to the maximum ion density recorded by the Faraday cup because the hydrogen line emission is too weak. However, the Faraday-cup measurement suggests that n_e may be a factor-of-two larger about 3 μs later (see Fig. 7).

The electron temperature, T_e, was inferred from the relative intensities of the CI line at 2478 Å and the CII lines at 2509-2512 Å. The relative populations of these ionization states of carbon can be calculated with the Saha equation for a plasma in local thermodynamic equilibrum (LTE) if both n_e and T_e are known.[16] Then, the relative population of the upper states of these two transitions is determined using the Boltzmann relationship for level populations. Oscillator strengths[17] of 0.094 for the $2p^2$-2p3s transition of CI and 0.14, 0.16, and 0.014 for the $2s2p^2$-$2p^3$ transitions of CII (J-J' = 3/2-5/2, 1/2-3/2, 3/2-3/2) were used to evaluate the relative intensity of these lines as a function of n_e and T_e. Because this line ratio depends on both T_e and n_e, T_e was determined only over the time interval for which n_e was also determined, as described in the previous paragraph. For the time interval from 2.25 to 5.25 μs, T_e = 1.4 - 1.6 eV. This measurement represents an upper limit on T_e because the weak CII line intensity may be over-estimated due to other contributions to this signal.

The plasma conditions required for LTE of the CI and CII ionization states and for equilibrium between these ionization states were examined. For a particular ionization state in a homogeneous static plasma, complete LTE is established if the collisional excitation rate is a factor of ten larger than the radiative decay rate of the resonance transition.[18] Applying this criterion to a 1.5-eV carbon plasma leads to lower limits on n_e of 5×10^{16} cm^{-3} for CI and 4×10^{17} cm^{-3} for CII. Thus, complete LTE is valid at the the time of measured peak n_e (8×10^{16} cm^{-3}) for CI but not for CII. Partial LTE with respect to transitions from higher principle quantum number does not require as large a density as complete LTE. If an effective principle quantum number of 3 is used for the CII transition,[18] partial LTE is valid because the minimum density is only 1×10^{16} cm^{-3}. The time required for equilibration between these ionization stages of carbon was estimated from inverse reaction rates.[19] An ionization rate coefficient of 8×10^{-12} cm^3/s, based on a 1.5-eV CI plasma, indicates an equilibration time of 1.5 μs for an electron density of 8×10^{16} cm^{-3}. For a plasma that goes through a sequence of near LTE states, the time required for relaxation of transient effects can be estimated from the inverse collisional excitation rate of the ground state multiplied by the fraction of atoms to be excited. This time is < 11 ns for CI. These comparisons suggest that the LTE analysis is marginally appropriate for the CI and CII states used for the temperature estimates.

A model[20] based on the Saha equation, charge neutrality, and conservation of particles was used to estimate the population of various ionization stages of sodium and fluorine in the plasma assuming a total density for each species of 10^{17} cm^{-3}. This density was selected because it leads to an electron density at 1.5 eV that is comparable with the measured n_e. The populations of each ionization state relative to the particular species, NaI, NaII, FI, and FII, are given in Fig. 19 as a function of plasma temperature. At the measured

temperature of $\lesssim$ 1.5 eV, the sodium is almost entirely ionized and the fluorine is 86% neutral. At 1.5 eV, populations of the discharge constituents are approximately 1% NaI, 49% NaII, 43% FI, and 7% FII. The population of F^- ions is negligible and becomes significant only for temperatures less than 0.6 eV. The population of NaIII is negligible over the temperature range in Fig. 19 due to the large ionization potential (47 V) of neonlike sodium.

The total particle density in the plasma was determined by combining the electron density with the population fractions deduced from the Saha model. This procedure is appropriate because the population fractions are only weakly dependent on the electron density. With only single-stage ionization, the value of n_e (8×10^{16} cm^{-3}) determined from the hydrogen line width is the total positive-ion density at the exit of the nozzle. This result is more than an order-of-magnitude larger than the density determined from the Faraday cup located 5-cm in front of the nozzle (see Section IV). This difference may result from expansion and/or recombination as the plasma expands away from the nozzle. For a total positive-ion density of 49% NaII and 7% FII, the total density (sodium and fluorine) is approximately 1.4×10^{17} cm^{-3}. This result is relatively insensitive to the temperature in the range from 0.7 to 1.6 eV because the sodium is more than 90% singly ionized for temperatures greater than 0.7 eV, and the FII contribution is less than 12% for temperatures below 1.6 eV. For a 2-cm diameter nozzle, this total density corresponds to a mass per unit length of 15 μg/cm at 4 μs after the start of the current (peak electron density in Fig. 18). This mass may be a factor-of-two larger 3 μs later in the current pulse.

The NaI density of 1.4×10^{15} cm^{-3}, based on impurity-line emission and the Saha-equation analysis, is not inconsistent with the minimum ground-state density of 3×10^{16} cm^{-3} estimated from absorption at line center of the 2852-Å line of NaI. These densities are obtained at different times and possibly at

different radial sites within the plasma at the exit of the nozzle. The smaller density is recorded at 4 μs (peak of n_e in Fig. 18), while the larger density is not observed until at least 6 μs after the discharge is initiated. Because both measurements are averaged along a radial line-of-sight through the plasma, the emission may occur at a different location in the plasma than the absorption occurs due to radial nonuniformities, as observed in Fig. 10.

VII. CONCLUSIONS

A sodium fluoride plasma for Z-pinch implosions has been produced from a capillary-discharge source. The capillary is driven with peak currents of 40 to 50 kA for a few microseconds to produce the plasma. Approximately 180 J of energy is delivered to the capillary to produce a plasma of sodium and fluorine which is ejected from the capillary. Nozzles are necessary to confine the plasma to a cylindrical geometry, either 1.2 to 2-cm in diameter. Ions are ejected at velocities of 2.2 to 3.4 cm/μs and neutrals at velocities of 1.5 to 1.7 cm/μs. Plasma is emitted for several microseconds so that a 4-cm length may be filled with plasma as required for Z-pinch implosion experiments.[6]

The plasma has nonuniformities in both the radial and axial directions. Measurements suggest that the plasma is emitted in successive fronts which may be associated with the periodic nature of the driving current. It may be possible to smooth these nonuniformities by using a slower-period current. Visible-light framing photographs suggest that the radial nonuniformities are due to reflection of plasma from the walls of the nozzle and from radial expansion of the plasma as it propagates away from the nozzle. Observed broadening of spatially-resolved spectral lines is consistent with a higher electron density on axis, particularly for the 2-cm diameter nozzle. Reducing the nozzle diameter seems to smooth the radial variations by producing a more uniform electron density throughout the plasma. Copper impurities in the plasma

originate from both electrodes of the capillary, and the impurities can be altered by changing the composition of the metal electrodes.

Time-resolved spectral-intensity measurements from carbon and hydrogen impurities were made to determine the electron density and temperature. An electron density of about 8×10^{16} cm^{-3} at the exit of the nozzle was determined from Stark broadening of optically-thin hydrogen-line emission. Temperatures of 1.4 to 1.6 eV were inferred from the relative intensity of CI and CII line emissions. Interpretation of these results with a Saha model indicates that the plasma consists mainly of NaII and FI at the exit of the nozzle, and a total (sodium and fluorine) density of about 1.4×10^{17} cm^{-3} is deduced from the electron density. Faraday-cup measurements 5 cm in front of the nozzle indicate that this density may be a factor-of-two larger a few microseconds later in time. This density represents a mass loading of 15 $\mu g/cm$ which compares favorably with values of 14 to 33 $\mu g/cm$ that have been inferred from observed implosion times[6] and analyses of spectroscopic measurements[21] in experiments with this source on the Gamble II pulsed power generator.

VIII. ACKNOWLEDGMENTS

We are grateful to R. Boller and G. Cooperstein of the Naval Research Laboratory (NRL) for their suggestions and to A.T. Robinson and G. Langley for technical assistance. We are grateful to M.J. Herbst (NRL) for making available the photodiodes used in these measurements. H.R. Griem, J.S. Wang, J. Moreno, E. Iglesias, S. Daniels, S. Goldsmith and R. Grober of the University of Maryland assisted in the interpretation and presentation of the spectral measurements. This work was supported in part by the Innovative Science & Technology Office of the Strategic Defense Initiative Organization and directed by the Naval Research Laboratory.

IX. REFERENCES

1. A.V. Vinogradov, I.I. Sobel'man, and E.A. Yukov, Sov. J. Quant. Electron. 5, 59 (1975); R.H. Dixon and R.C. Elton J. Opt. Soc. Am. B1, 232 (1984).
2. V.A. Bhagavatula, Appl. Phys. Lett. 33, 776 (1981).
3. P. Rabinowitz, S. Jacobs, and G. Gould, Appl. Opt. 1, 513 (1962).
4. J.P. Apruzese and J. Davis, Phys. Rev. A31, 2976 (1985).
5. S.J. Stephanakis, J.P. Apruzese, P.G. Burkhalter, J. Davis, R.A. Meger, S.W. McDonald, G. Mehlman, P.F. Ottinger, and F.C. Young, Appl. Phys. Lett. 48, 829 (1986); and G. Mehlman, P.G. Burkhalter, S.J. Stephanakis, F.C. Young, and D.J. Nagel, J. Appl. Phys. 60, 3427 (1986).
6. F.C. Young, S.J. Stephanakis, V.E. Scherrer, B.L. Welch, G. Mehlman, P.G. Burkhalter, and J.P. Apruzese, Appl. Phys. Lett. 50, 1053 (1987).
7. S.J. Stephanakis, J.P. Apruzese, P.G. Burkhalter, G. Cooperstein, J. Davis, D.D. Hinshelwood, G. Mehlman, D. Mosher, P.F. Ottinger, V.E. Scherrer, J. W. Thornhill, B.L. Welch, and F.C. Young, IEEE Trans. Plasma Sci. 16, 472 (1988).
8. H.J. Kusch and H. Schreiber, Z. Naturforsh. 27, 513 (1972); and N.N. Ogurtsova, I.V. Podmoshenskii, and V.L. Smirnov, High Temp. 14, 1 (1976).
9. R.C. Cross, B. Ahlborn, and J.D. Strachan, J. Appl. Phys. 42, 1221 (1971); and D.D. Hinshelwood and Shyke A. Goldstein, in Record 1981 IEEE Inter. Conf. Plasma Sci. (Santa Fe, New Mexico, May 1981), p. 83.
10. S.M. Zakharov, A.A. Kolomenskii, S.A. Pikuz, and A.I. Samokhin, Sov. Tech. Phys. Lett. 6, 486 (1980).
11. R.A. McCorkle, Nucl. Instrum. Meth. 215, 463 (1983).
12. F.C. Young, R.J. Commisso, G. Cooperstein, D.D. Hinshelwood, R.A. Meger, D. Mosher, V.E. Scherrer, S.J. Stephanakis, B.V. Weber, and B.L. Welch, in Record 1986 IEEE Inter. Conf. Plasma Sci. (Saskatoon, Canada, May 1986), p.87.

13. H.R. Griem, Spectral Line Broadening by Plasmas, (Academic Press, New York, 1974).

14. B.L. Welch, H.R. Griem, R.J. Commisso, and F.C. Young, in Record 1987 IEEE Inter. Conf. Plasma Sci. (Arlington, VA, June 1987) p. 70.

15. D.H. Oza and R.L. Greene, J. Phys. B: At. Mol. Opt. Phys. 21, L5 (1988).

16. H.R. Griem, Plasma Spectroscopy, (McGraw-Hill, New York, 1964) p. 272.

17. W.L. Wiese, M.W. Smith, and B.M. Glennon, Atomic Transition Probabilities, 1, NSRDS-NBS 4 (US Government Printing Office, Washington, DC, 1966).

18. H.R. Griem, Plasma Spectroscopy, (McGraw-Hill, New York, 1964) p. 150.

19. W. Lotz, Ap. J. Suppl. 14, 207 (1967).

20. S.W. Daniels, H.R. Griem, and A.D. Krumbein, Proc. Third Inter. Conf. on Radiative Properties of Hot Dense Plasma, B. Rozsnyai, C. Hooper, R. Cauble, R. Lee, and J. Davis, Eds., (World Scientific Publ. Co., Singapore, 1985) p. 451.

21. J.P. Apruzese, G. Mehlman, J. Davis, J.E. Rogerson, V.E. Scherrer, S.J. Stephanakis, P.F. Ottinger, and F.C. Young, Phys. Rev. A35, 4896 (1987).

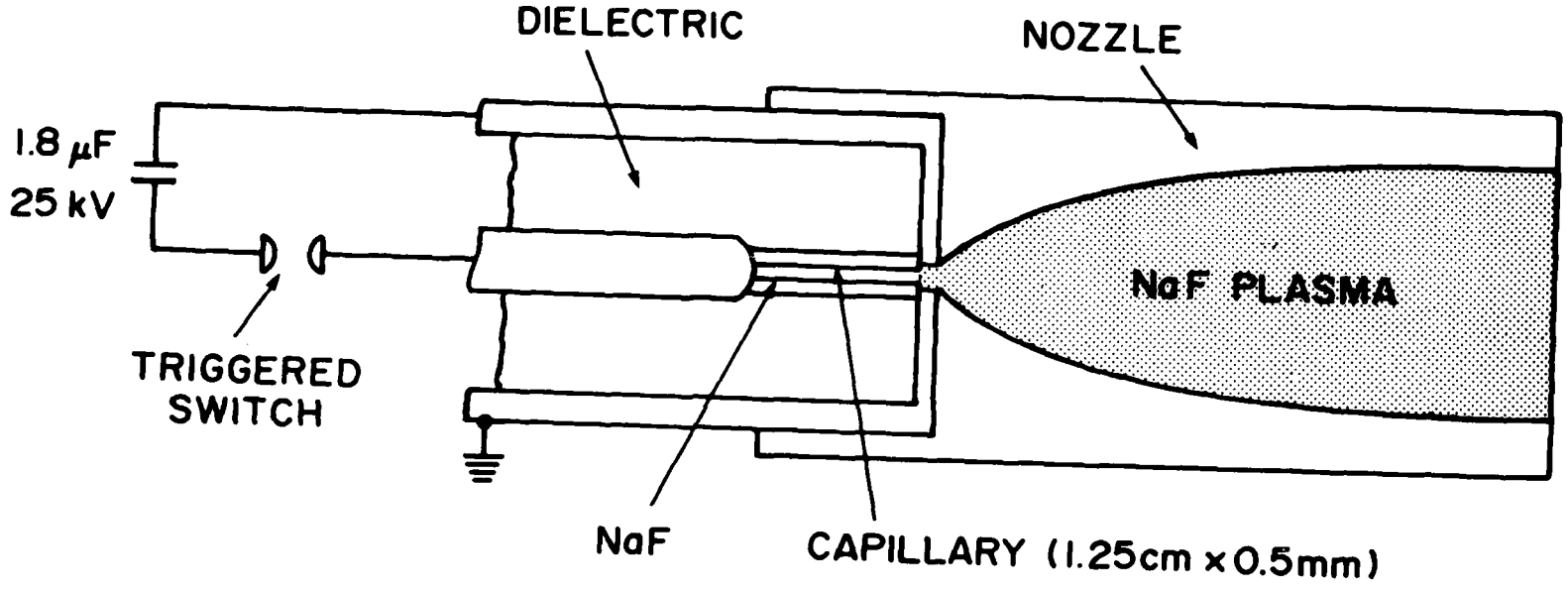

Fig. 1. Geometry of the sodium-fluoride capillary-discharge source.

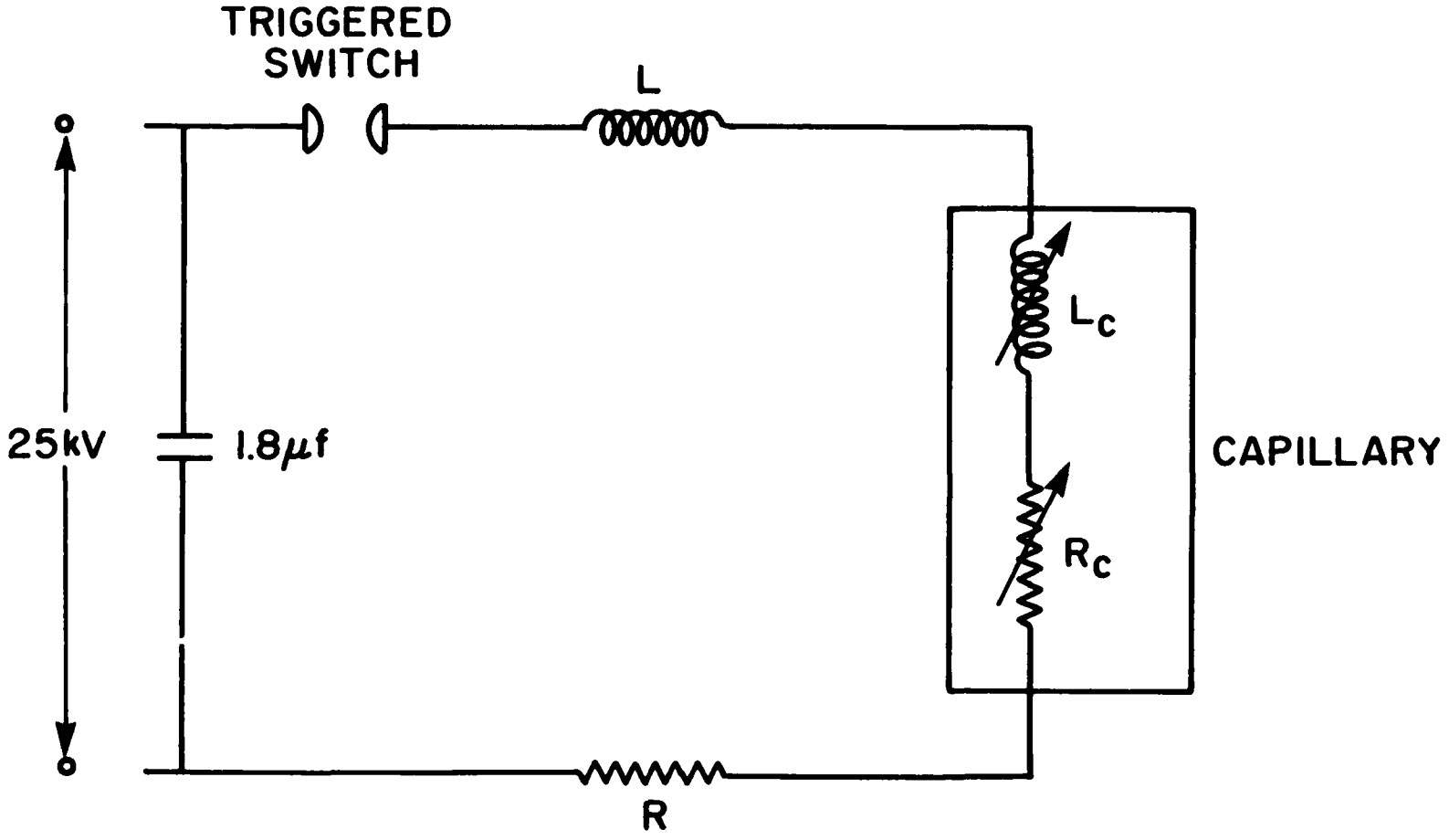

Fig. 2. Electrical circuit used to power the capillary.

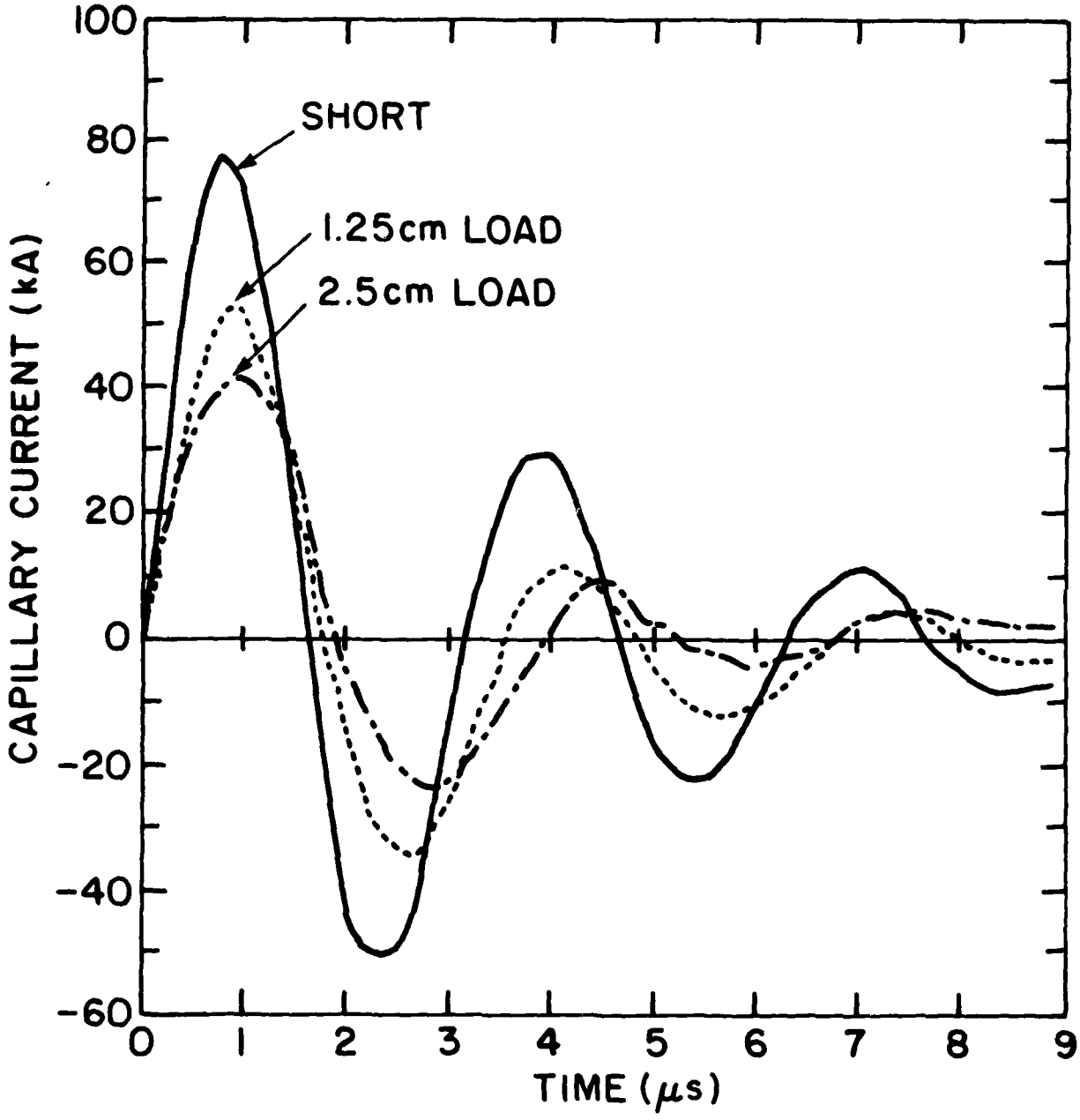

Fig. 3. Current traces for different capillary conditions.

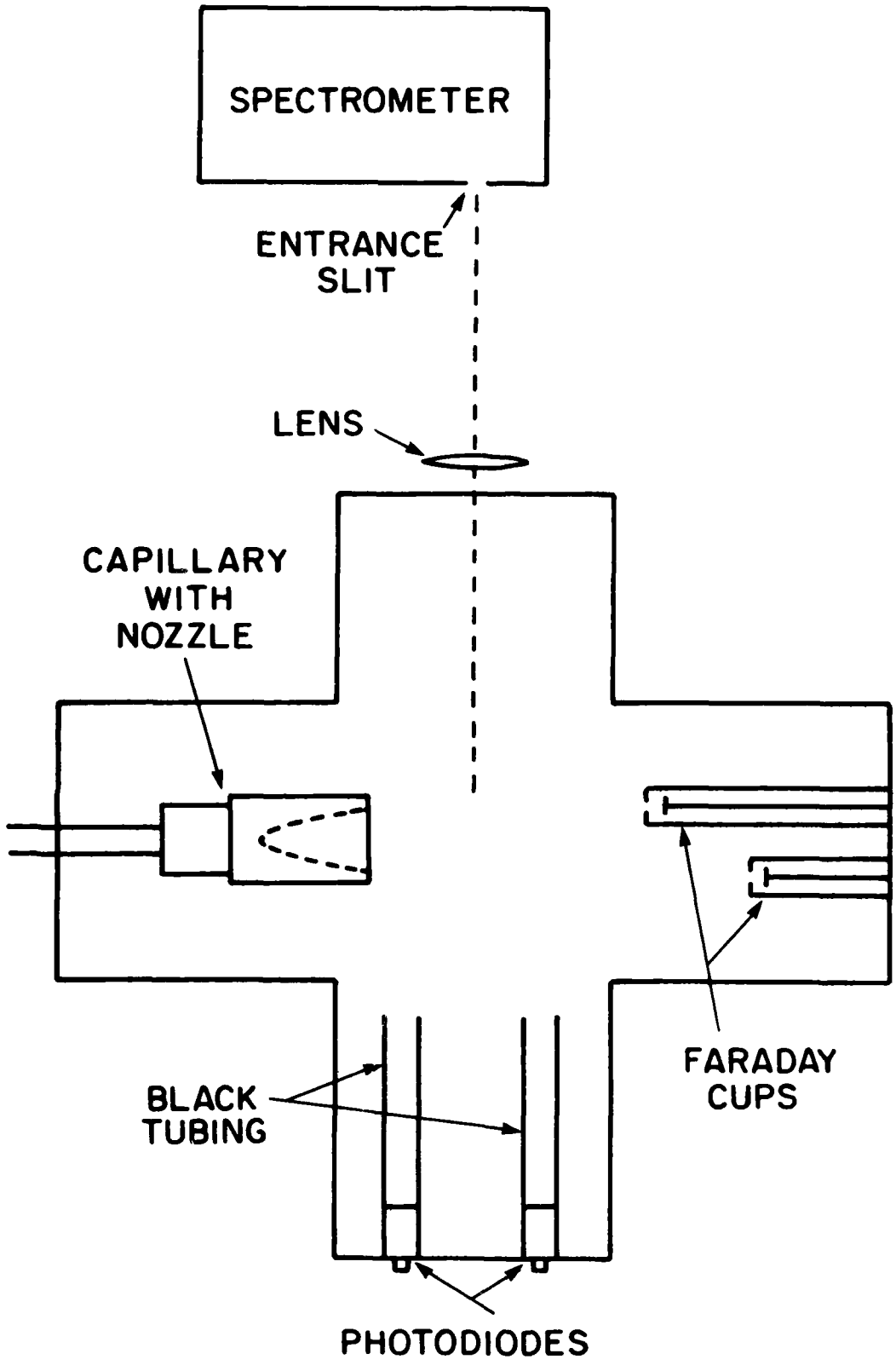

Fig. 4. Experimental arrangement of diagnostics on the capillary source.

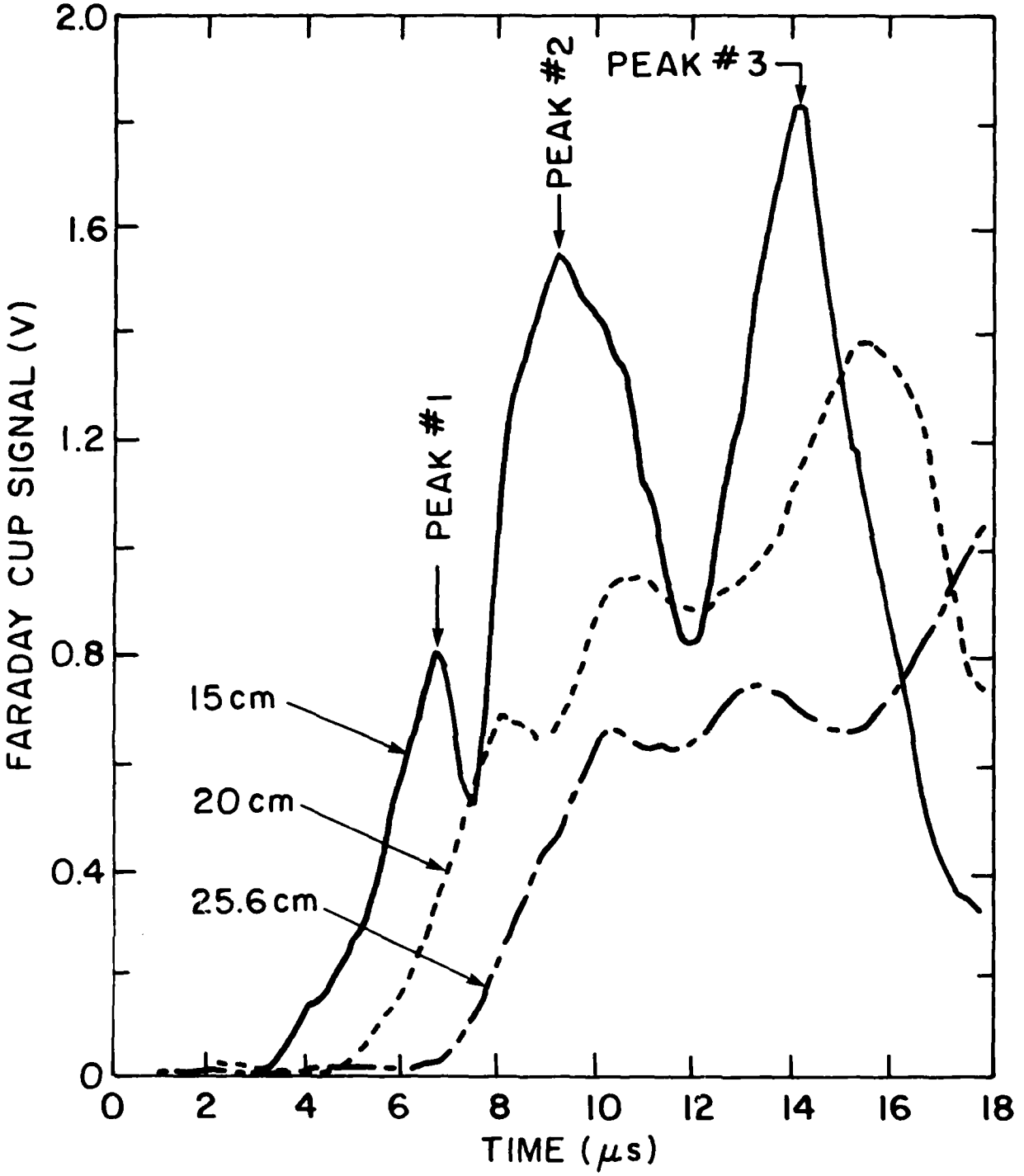

Fig. 5. Signals from a Faraday cup located 15 cm from the nozzle on one shot and from Faraday cups located 20 and 25.6 cm from the nozzle on another shot.

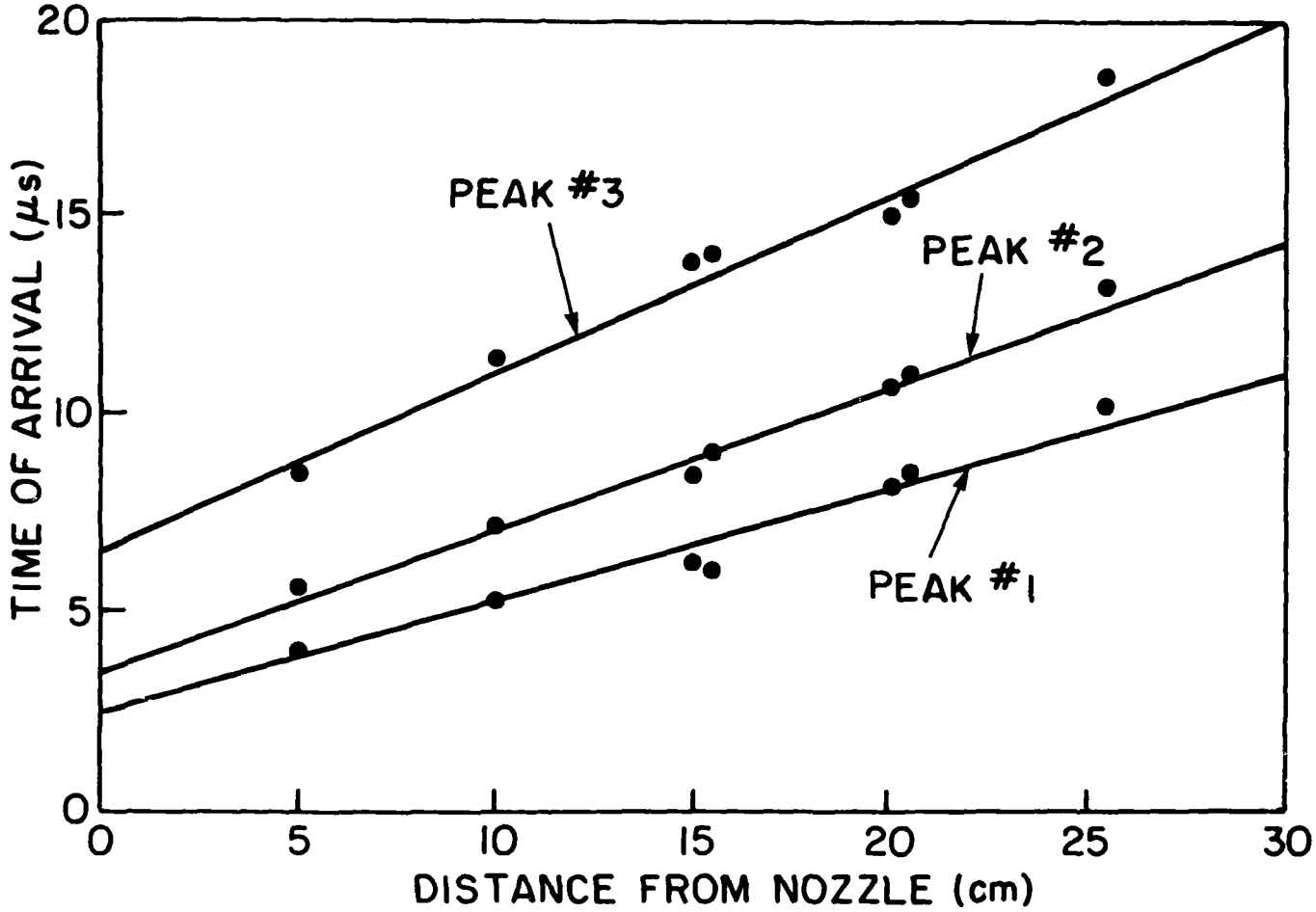

Fig. 6. Plot of the time of arrival for the peaks of the Faraday-cup signals in Fig. 5 versus the distance from the nozzle. The lines are least-square fits to the data.

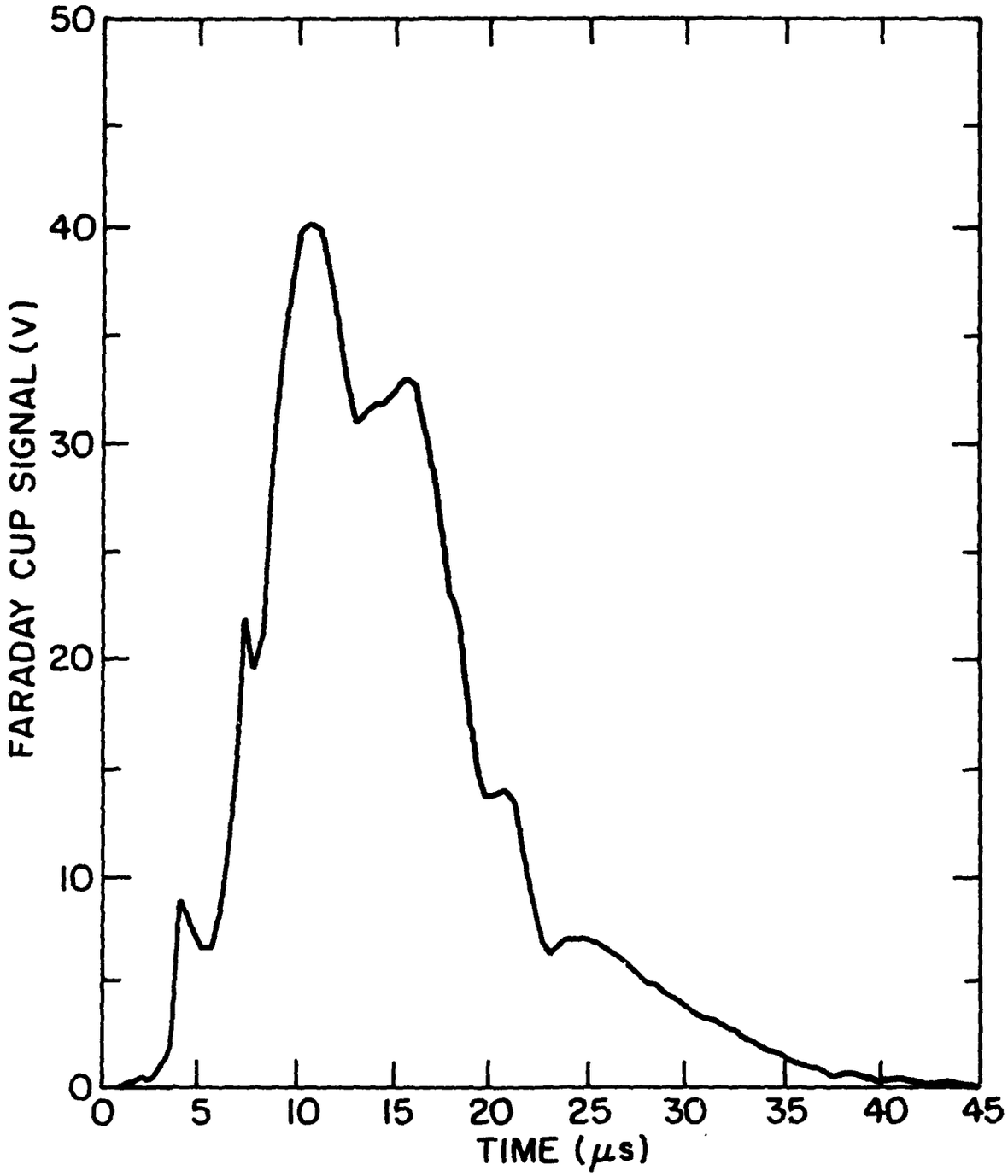

Fig. 7. Faraday-cup signal measured at 5 cm from a 2-cm diameter nozzle for a 2.5-cm long NaF capillary.

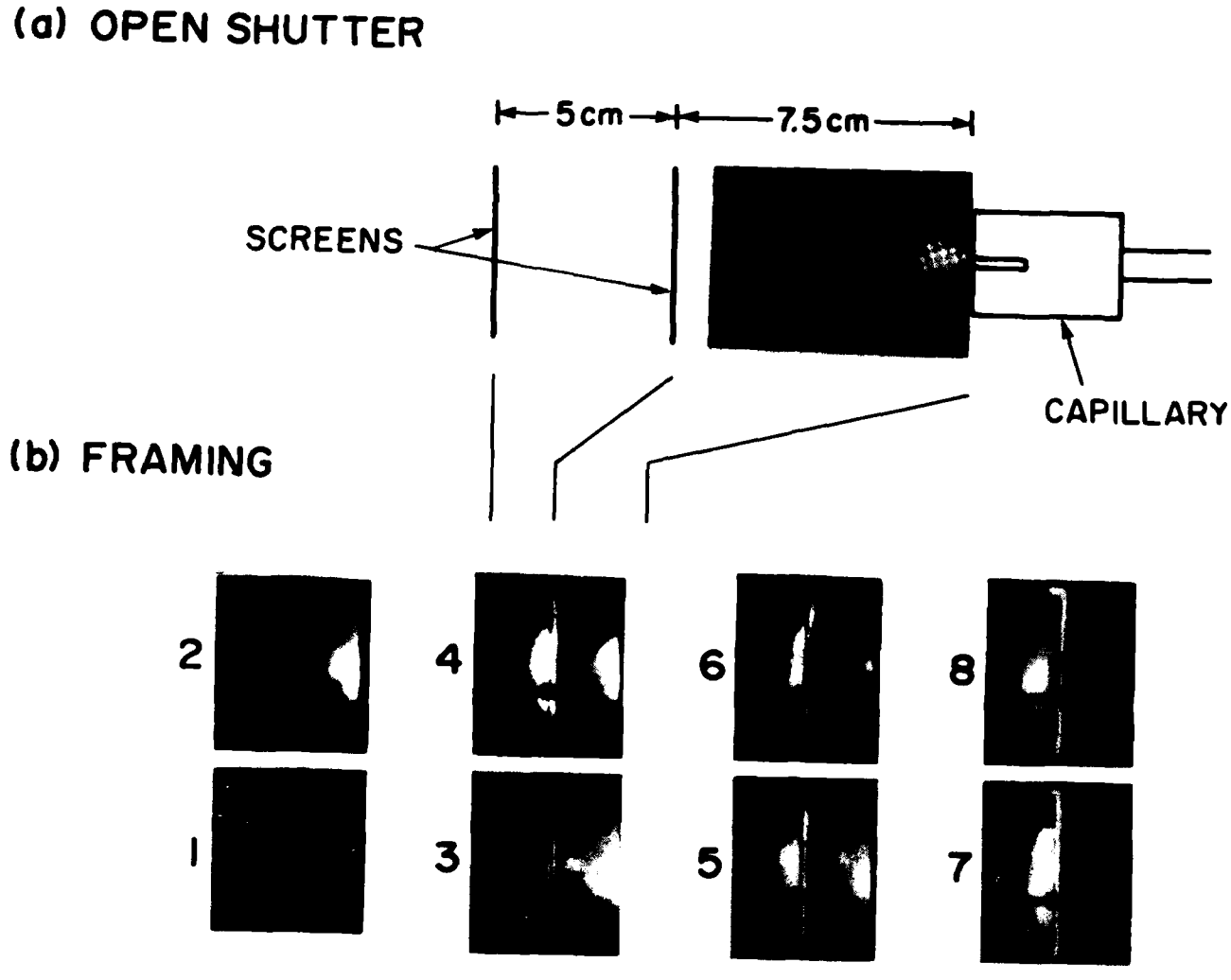

Fig. 8. (a) Time-integrated photograph of sodium "doublet" light for a 1.25-cm long NaF capillary, and (b) framing-camera pictures with no light filter for a 1.25-cm long CF_2 capillary.

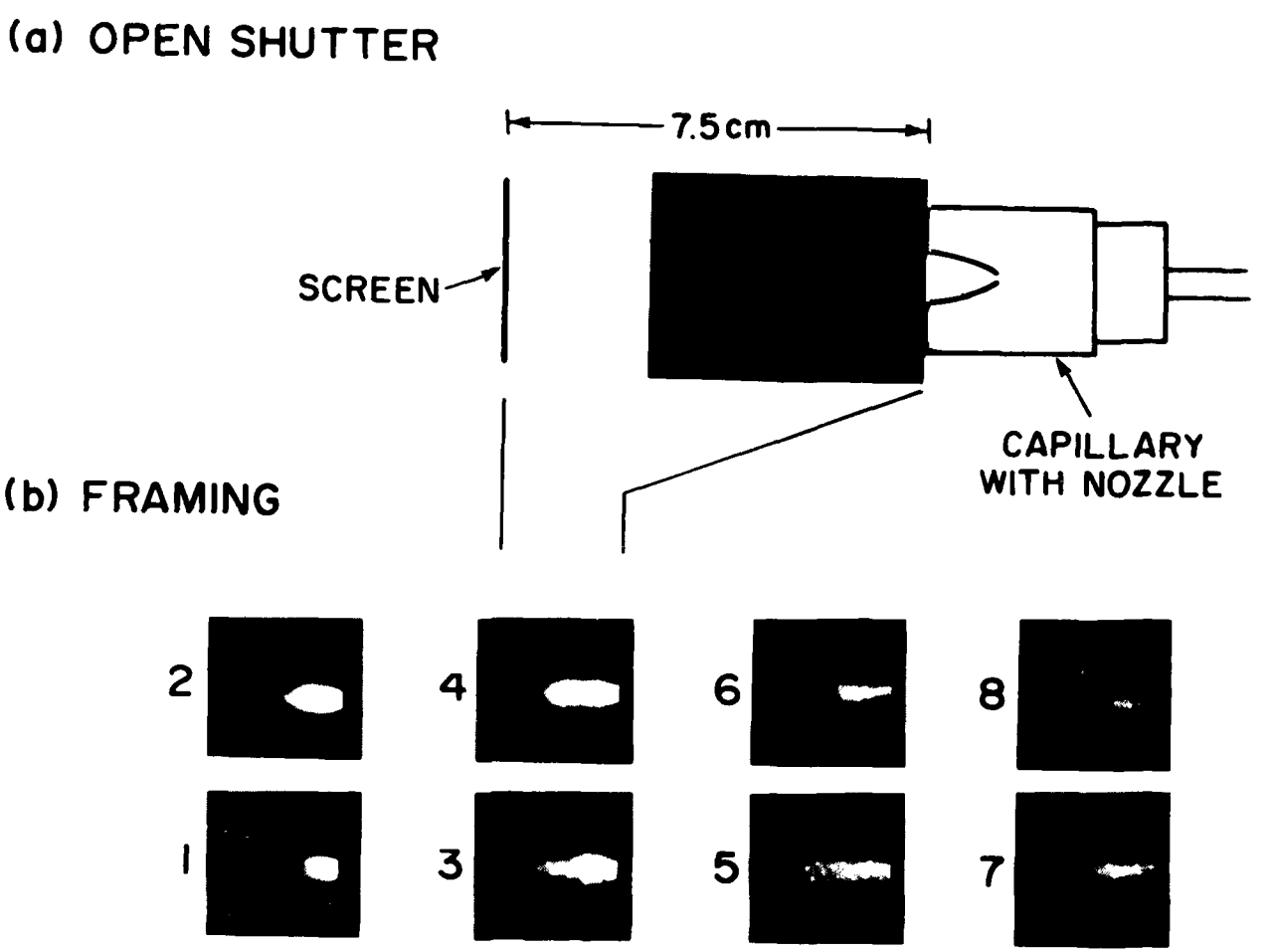

Fig. 9. (a) Time-integrated photograph and (b) framing-camera pictures for a 1.25-cm long NaF capillary with a 1.2-cm diameter, 2-cm long nozzle.

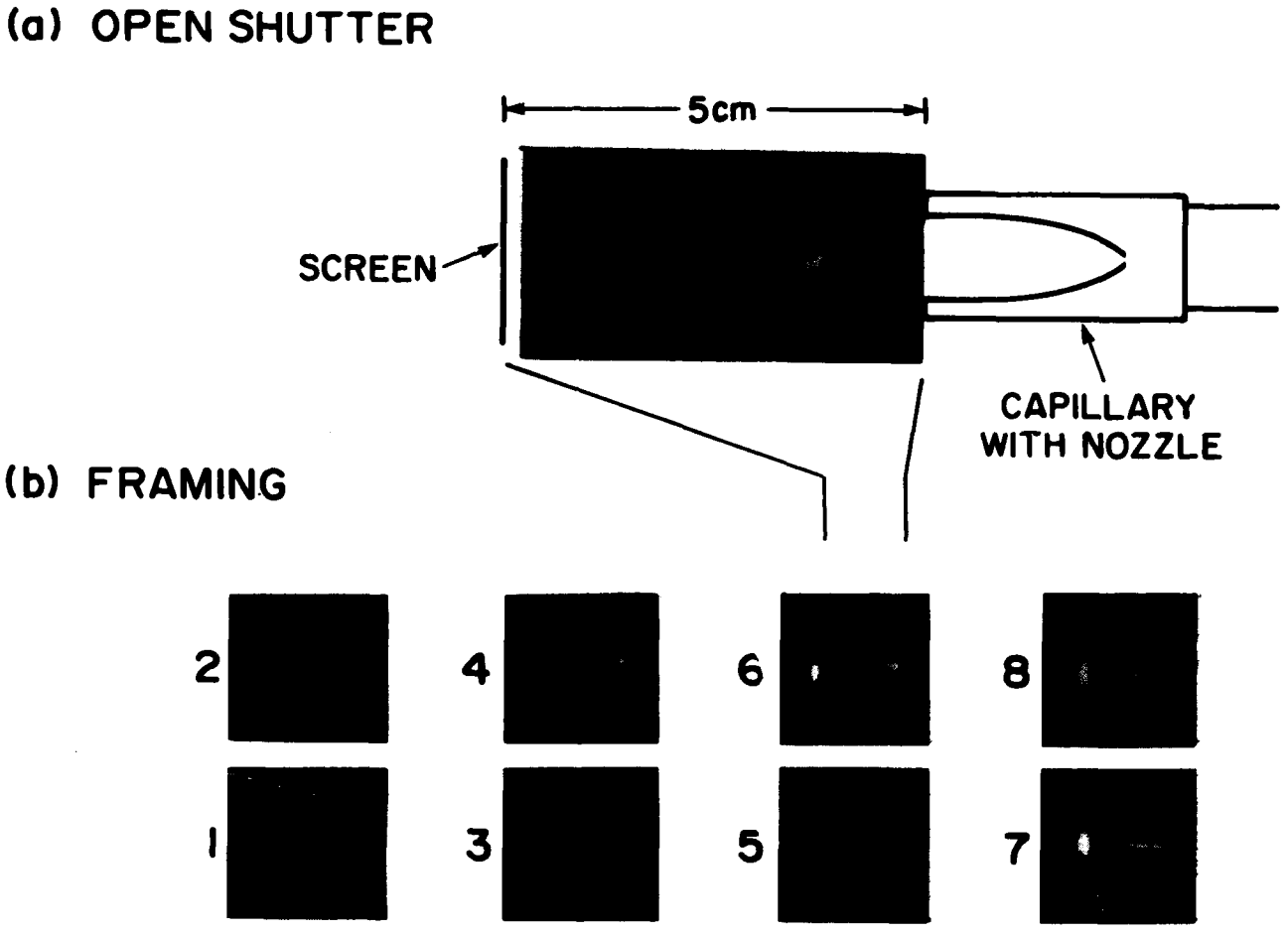

Fig. 10. (a) Time-integrated photograph and (b) framing-camera pictures for a 1.25-cm long NaF capillary with a 2-cm diameter, 5-cm long nozzle.

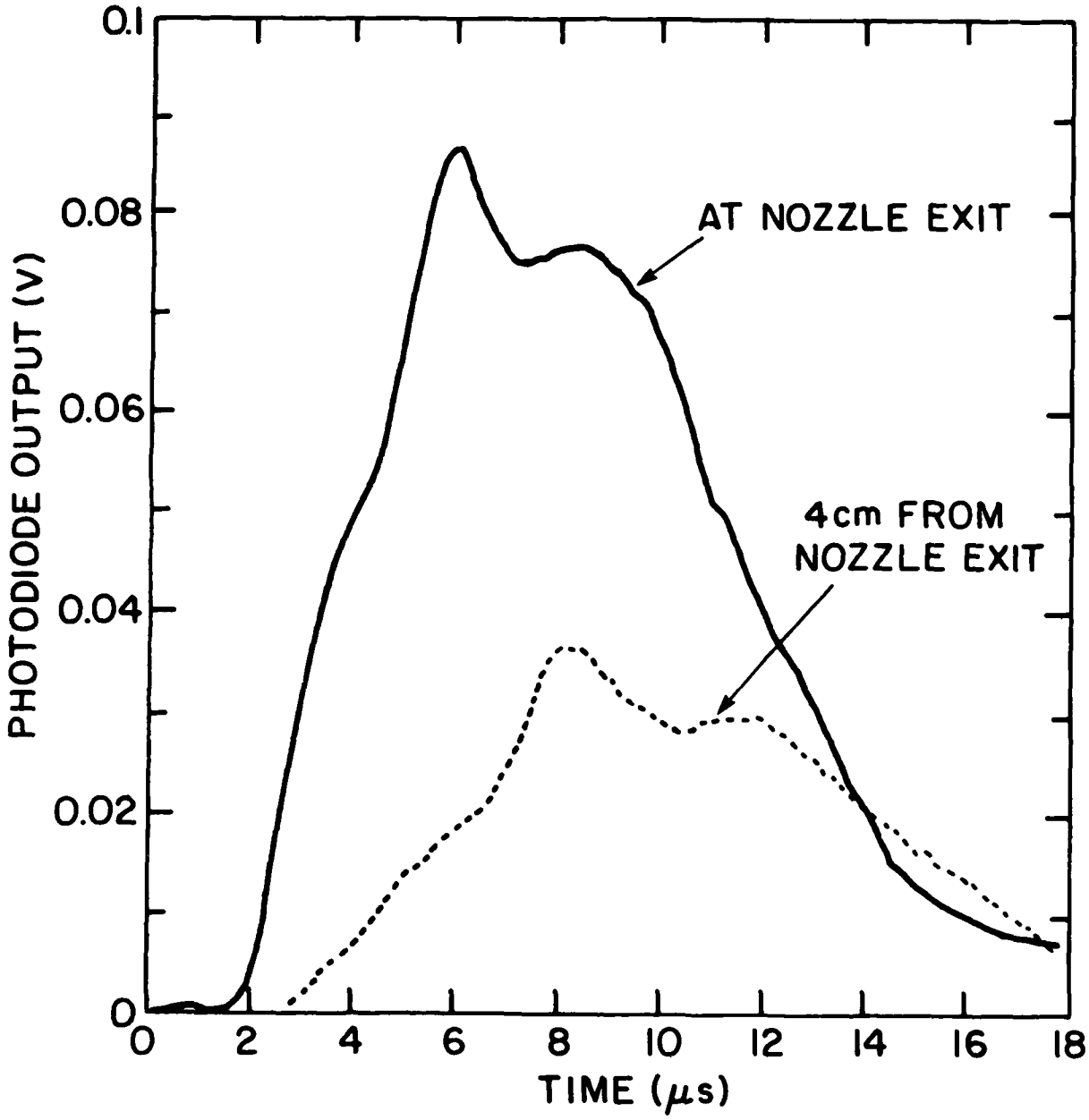

Fig. 11. Photodiode signals for a 1.25-cm long NaF capillary measured at the exit of a 2-cm diameter nozzle (solid) and at 4 cm from the nozzle (dash).

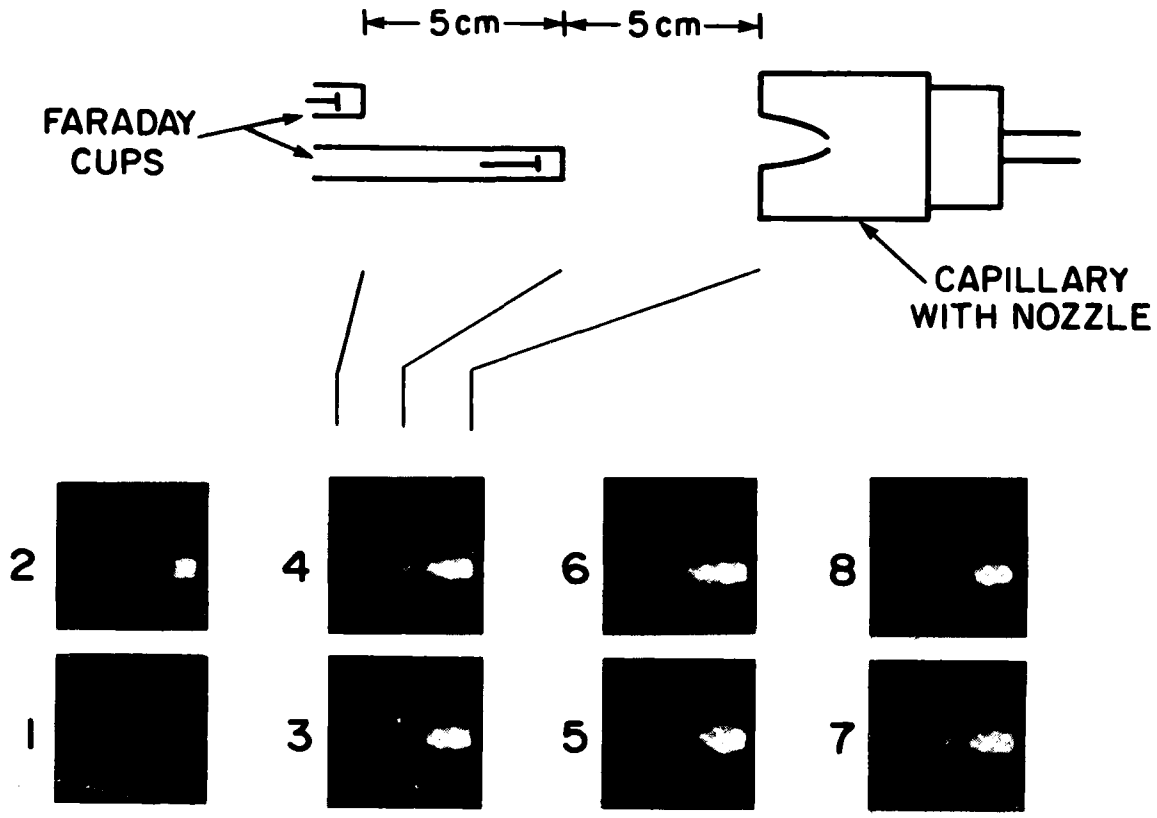

Fig. 12a — Framing-camera pictures for a 1.25-cm long CF_2 capillary with a 1.2-cm diameter, 2-cm long nozzle. Faraday cups were located 5 and 10 cm from the nozzel.

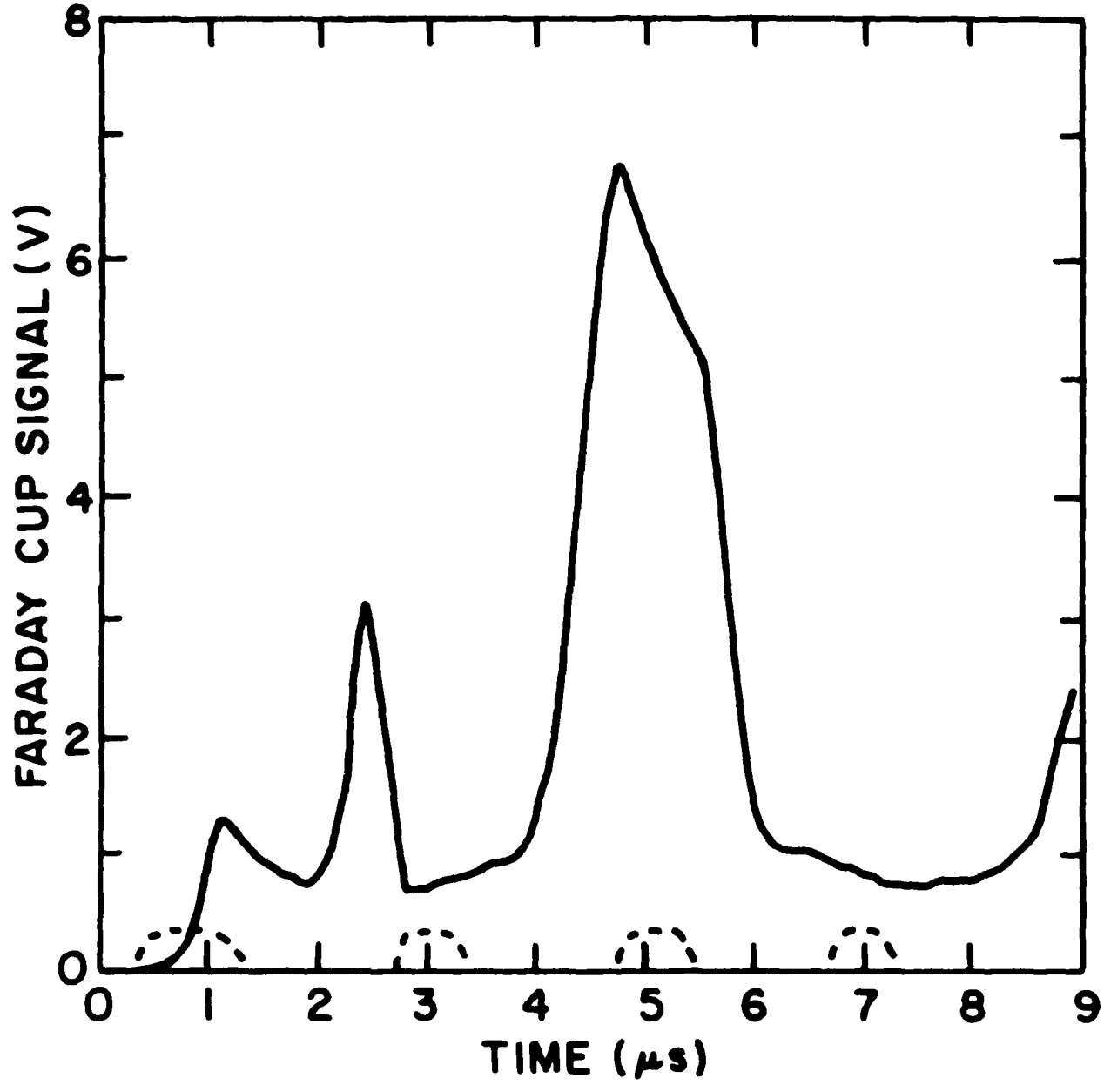

Fig. 12b — Faraday cup signal (solid) for the detector in Fig. 12a located 5 cm from the nozzel. The dashed curve shows the frame-times corresponding to the bottom row of framing pictures in Fig. 12a.

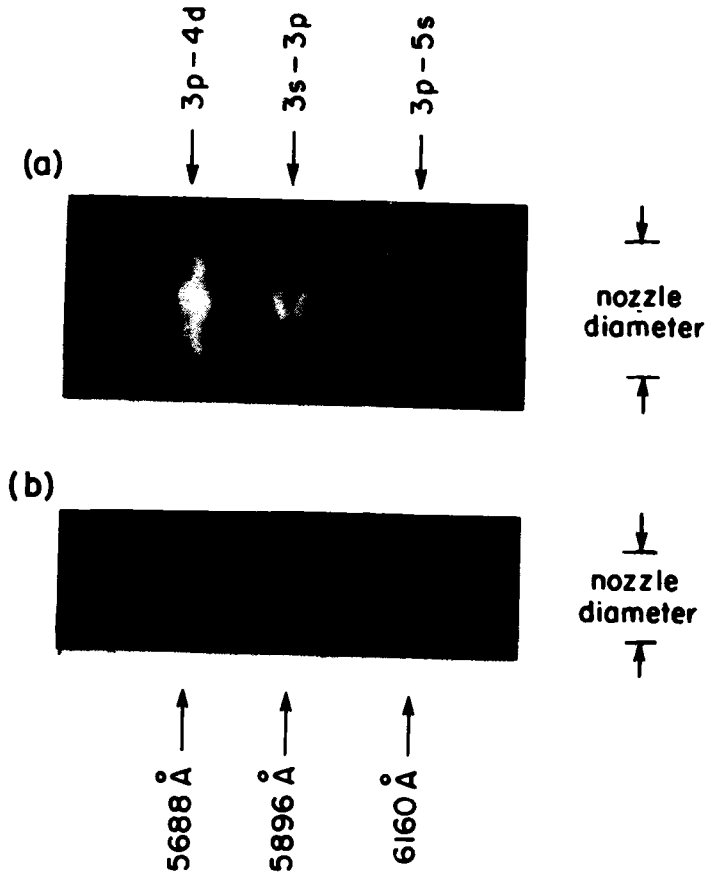

Fig. 13. Spectral lines from NaI for a 1.25-cm long NaF capillary (a) with a 2-cm diameter nozzle and (b) with a 1.2-cm diameter, 5-cm long nozzle. The short lines along the bottom of the photographs are reference spectra.

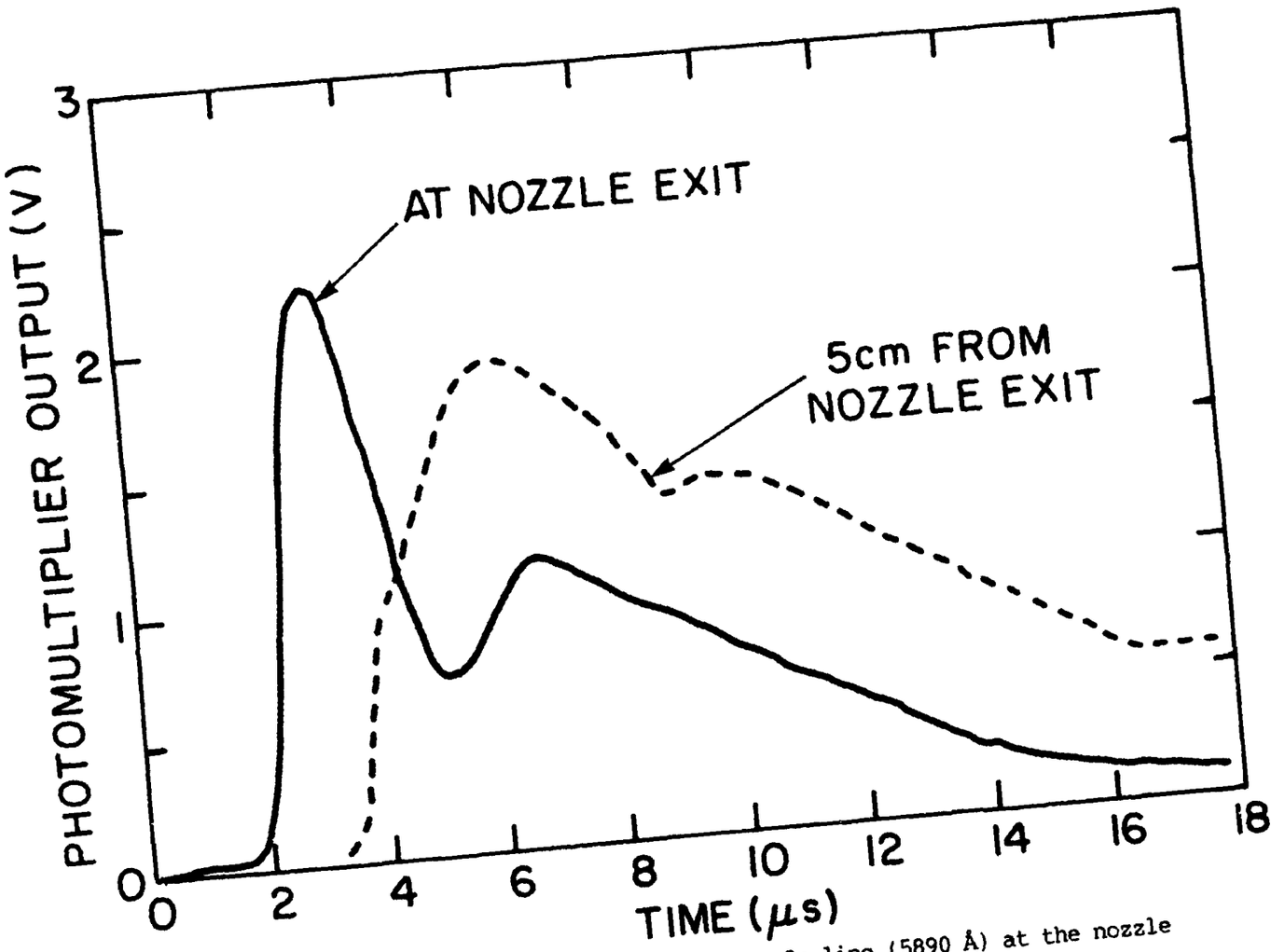

Fig. 14. Photomultipler signals of the NaI 3s-3p line (5890 Å) at the nozzle exit (solid) and 5 cm from the nozzle (dash) for a 2.5-cm long NaF capillary and 2-cm diameter nozzle.

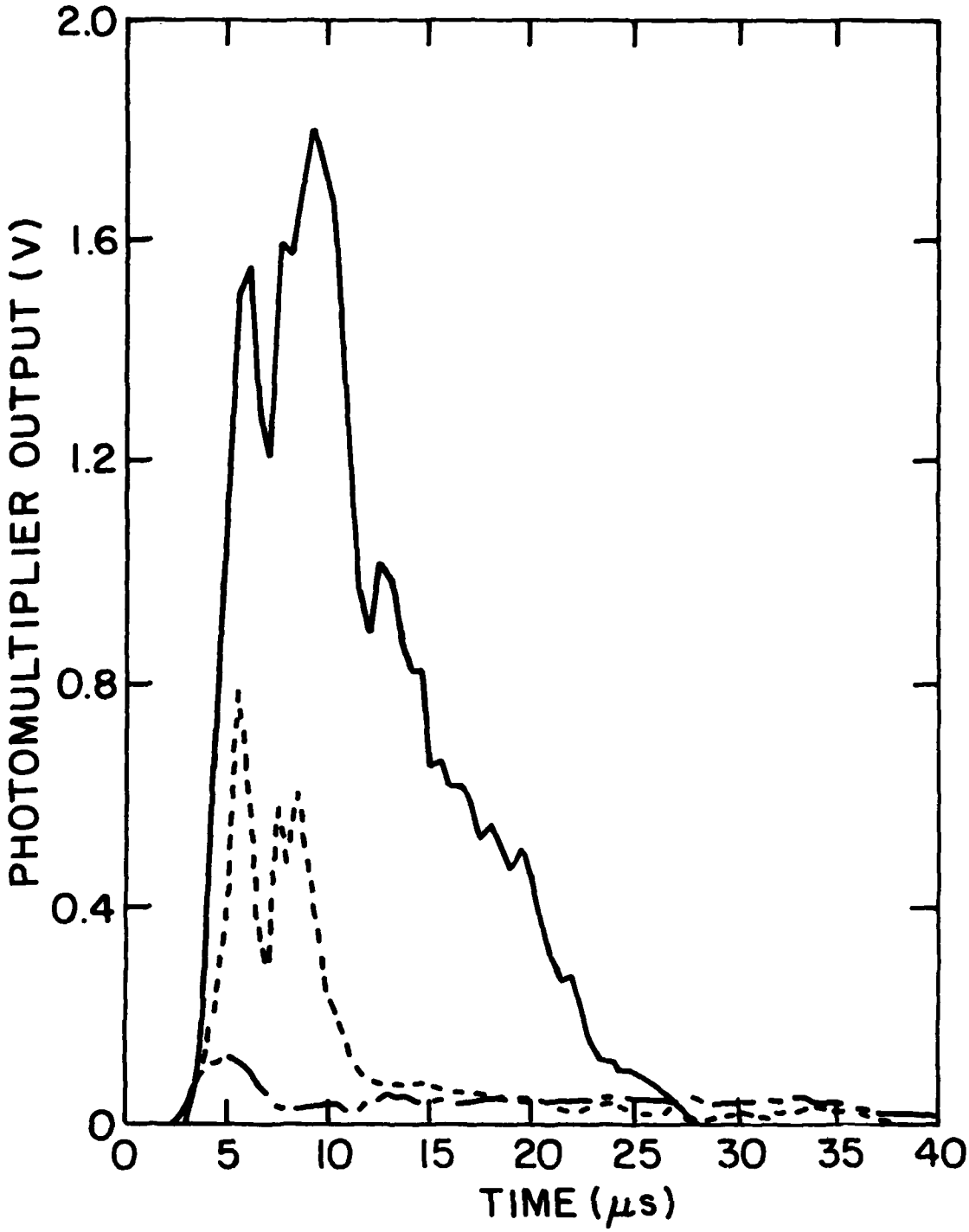

Fig. 15. Photomultiplier signals of the 5218-Å CuI line for a 2.5-cm long NaF capillary and 2-cm diameter nozzle with brass electrodes (solid), with an aluminum outer electrode (short dash), and with an aluminum outer electrode and tantalum inner electrode (long dash).

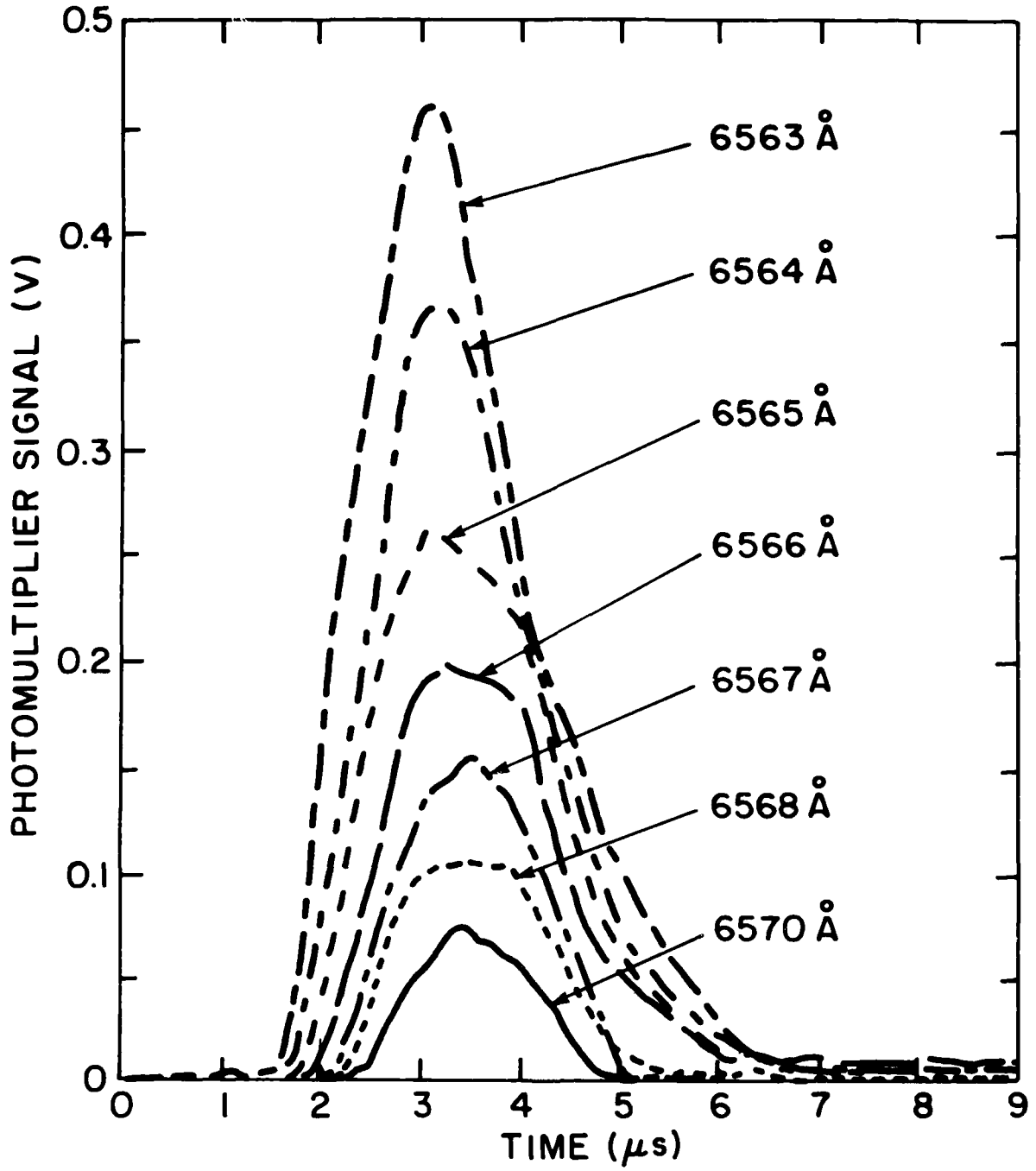

Fig. 16. Photomultiplier signals of the Balmer alpha line of hydrogen at line center (6563 Å) and at six longer wavelengths for a 1.25-cm long NaF capillary with a 2-cm diameter nozzle.

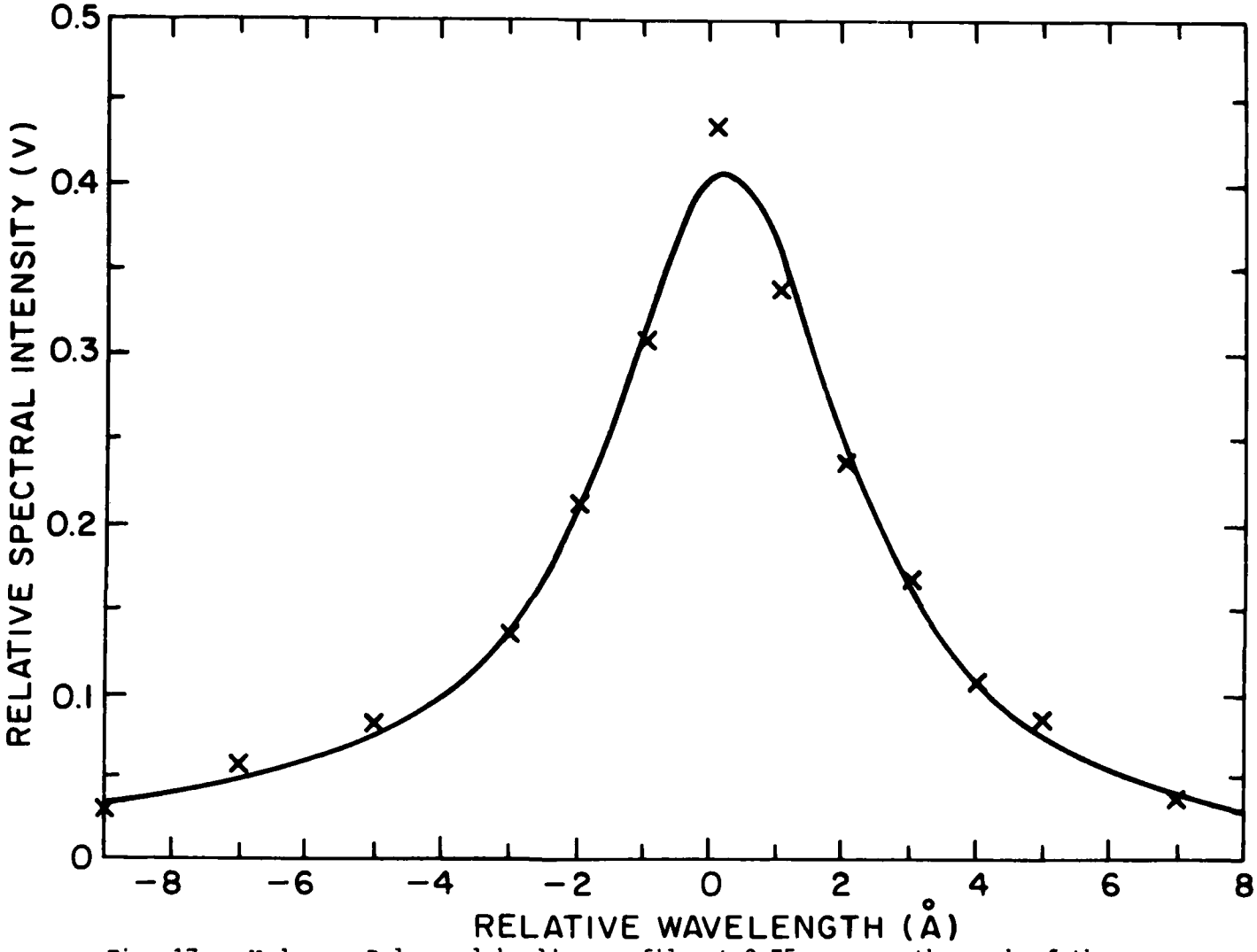

Fig. 17. Hydrogen Balmer alpha line profile at 2.75 μs near the peak of the signals in Fig. 16. Zero on the horizontal axis corresponds to line center. The curve is the fit of a Lorentzian function with a linear background.

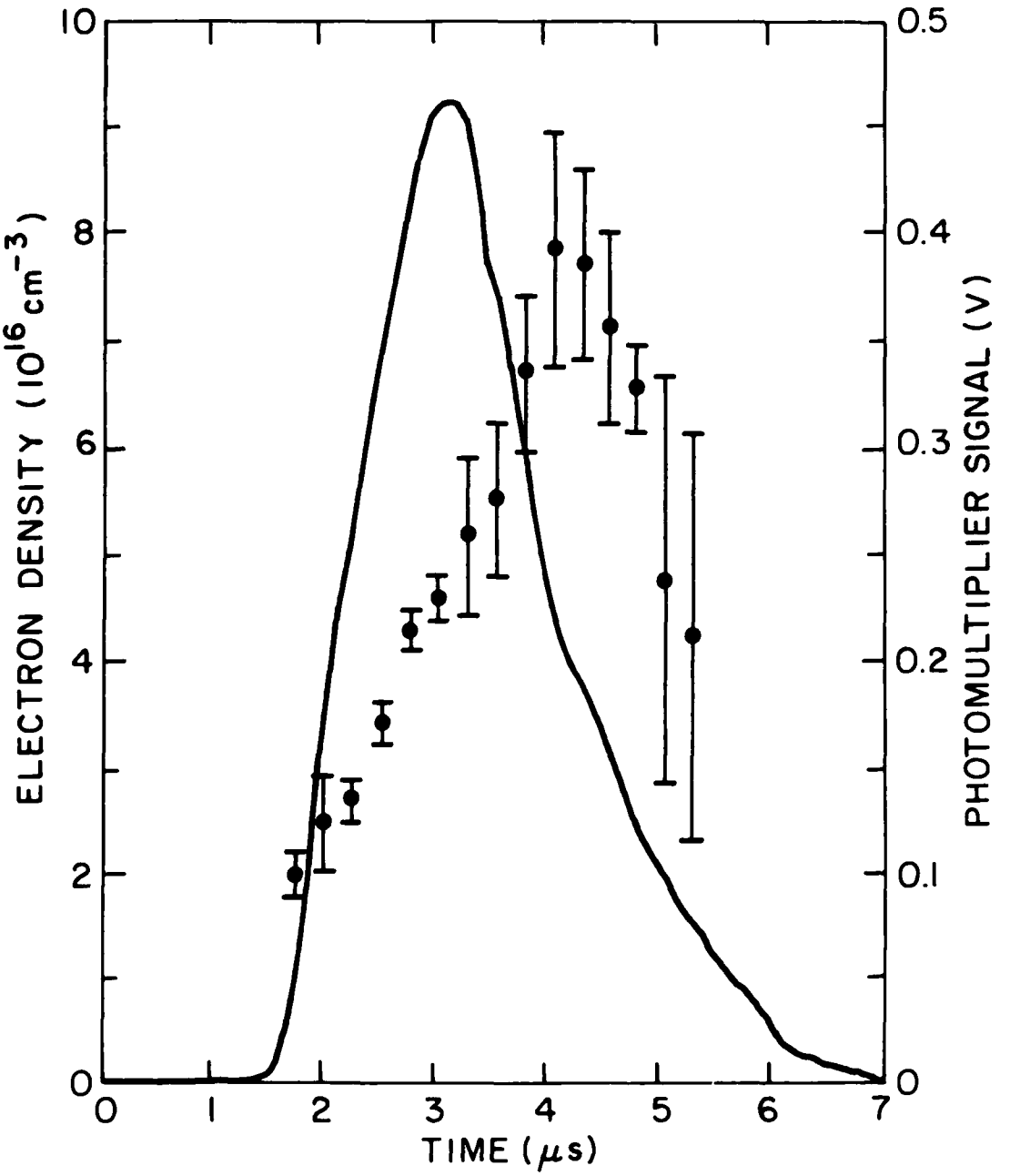

Fig. 18. Electron densities determined from the measured line widths (data points), and the photomultiplier signal of the Balmer alpha line of hydrogen at line center (curve).

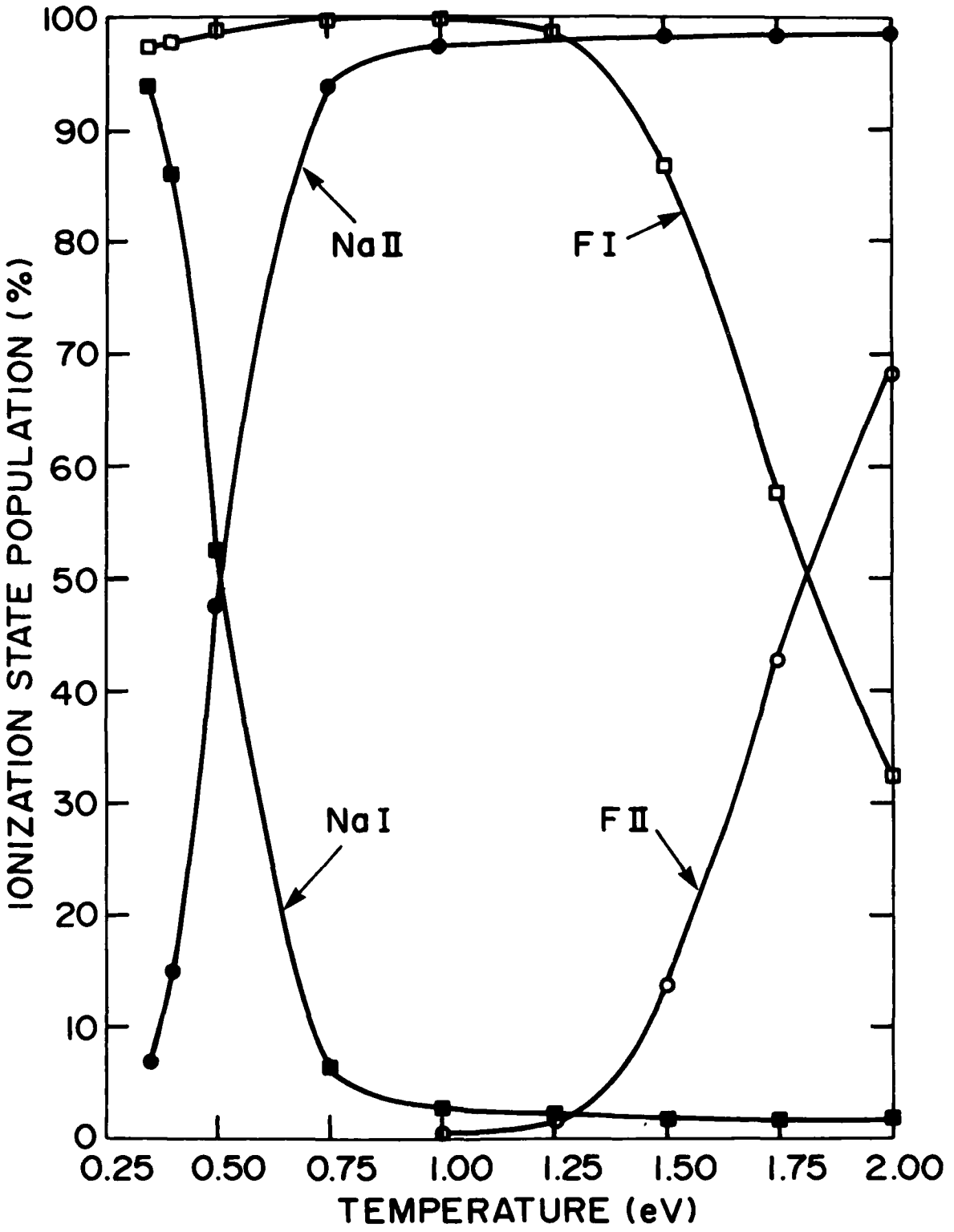

Fig. 19. Populations of the ionization states of sodium and fluorine for a NaF plasma with a total ion density of 2×10^{17} cm^{-3}.

DISTRIBUTION LIST

Naval Research Laboratory
Washington, DC 20375-5000
Attn: COTR Code 4720 — 2 copies
Contract Office 4702 — 1 copy
Office of Director 2627 — 6 copies
Code 1004 — 1 copy

Defense Technical Information Center
Building 5 Camerson Station
Alexandria, VA 22314 — 12 copies

Dr. Dwight Duston
SDIO/T/IS
Washington, DC 20301-7100 — 1 copy

Dr. Len Caveny
SDIO/T/IS
Washington, DC 20301-7100 — 1 copy

Lt. Col. Richard Gullickson
SDIO/T/DE
Washington, DC 20301-7100 — 1 copy

Captain David Dimiduk
SDIO/T/DE
Washington, DC 20301-7100 — 1 copy

Dr. Terry Kammash
The University of Michigan
Cooley Building, North Campus
Ann Arbor, MI 48109-2104 — 1 copy

Dr. Joseph Reader
Center for Radiation Research
U. S. Dept of Commerce
Gaithersburg, MD 20899 — 1 copy

Dr. Mahadevan Krishnan
Physics International
2700 Merced Street
San Leandro, CA 94577 — 1 copy

Dr. Steve Harris
Stanford University
Edward Ginzton Laboratories
Stanford, CA 94305 — 1 copy

Dr. Thomas F. Gallagher
University of Virginia
Department of Physics — 1 copy
McCormick Road
Charlottesville, VA 22901

Dr. Charles Rhodes
University of Illinois at Chicago
Department of Physics — 1 copy
Box 4348
Chicago, IL 60680

Dr. Baruch Yaakobi
University of Rochester
Laboratory of Laser Engergetics — 1 copy
250 East River Road
Rochester, NY 14623-1299

Dr. Simon Suckewer
Princeton University
Plasma Physics Laboratory
James Forrestal Campus — 1 copy
P.O. Box 451
Princeton, NJ 08544

Dr. Hans R. Griem — 1 copy
University of Maryland
College Park, MD 20742

Dr. Ira B. Bernstein
Yale University
Atomic & Plasma Radiation Division — 1 copy
Section of Applied Physics
New Haven, CT 06521-2159

A. E. Kingston
Professor of Theoretical Atomic Physics
The Queen's University of Belfast
Belfast BT7 INN Northern Ireland
1 copy

Dr. Gerald Cooperstein
Naval Research Laboratory
Code 4770
Washington, DC 20375-5000
1 copy

Dr. B. Klein
Naval Research Laboratory
Code 6680
Washington, DC 20375-5000
1 copy